Development of Highly Sensitive Label-Free Detection Method and its Practical Application Using Micro- and Nanofluidic Devices

Taiga AJIRI

Hokkaido University

Contents

Chapter 1.
General Introduction

1.1 Analysis of Biomolecules

In the early 19th century, enzymes were first discovered, and the study of biomolecules became an important field in science [1]. The number of molecules believed to exist in our surroundings is in the tens of thousands. Analyses of specific biomolecules, such as DNA, RNA [2-8], proteins [9-11], antigens [12-15], antibodies [16-18] and exosomes [19-22] are required for a variety of experimental, diagnostic, and therapeutic purposes. The Human Genome Project (HGP) was completed in 2003, and subsequently, due to the progress in various biomolecular analysis techniques and basic research involving DNA, transformations in medicine and drug discovery such as tailor-made medicine and oligonucleotide therapeutics discovery continue to occur [23-25]. The importance of preventive health care based on the prediction of diseases by genetic diagnoses or some other diagnoses is increasing [26]. To provide the latest medical and diagnostic techniques on a global scale, basic and application-based research studies remain necessary. To accelerate these studies, a highly sensitive technique to accurately analyze biomolecules using a wide variety of information is required.

Various biomolecules can be analyzed in a number of ways using the current technological innovations. Today, biomolecules have been analyzed at the single molecule level and can offer new information in the fields of medical science and biology [27-30]. Many of these techniques, however, require specific skills and, therefore, training. To improve the efficiency of these technologies, their processing times and throughputs must be increased.

1.2 Microfluidics and Nanofluidics

In 1990, A. Manz *et al*. proposed the concept of μTAS (micro total analysis systems) at Ciba-Geigy in Switzerland [31]. They proposed the integration of all the wet chemical and electrical detection technology required to perform laboratory measurements into a single, miniature system (device). Based on this concept, research projects have been conducted world-wide, and the operations required for bioanalysis that were previously performed in test tubes, flasks, and microtubes were integrated within the microchannels fabricated into the device [32-40]. These devices enable the high-speed, parallel processing, and automation operations. In these miniaturized devices, ease of use and advantages due to miniaturization were reported. Several common advantages of microfluidic devices are listed below.

1. The amount of sample used for operations can be reduced. This is important for manipulating precious samples such as biomolecules.
2. The specific surface area is increased. Surface tension can be used in the operation and measurement can be performed with a high S (Signal) / N (Noise) ratio by immobilizing the object on the surface to be measured or provide interaction area.
3. The flow within the microfluidic device is laminar. By using laminar flow, it is easy to transport to each flow channel without interference, and it is also easy to control the reaction within the channel.
4. Isolation is easy when dangerous reactions and reagents are used.
5. It is easy to dispose of waste or device.
6. It is easy for the mass production of devices incorporating semiconductor microtechnology or other technologies.

Many additional advantages are also provided by these devices. Based on these advantages, many research projects have been conducted, and the technology of microfluidics has progressed rapidly to the point where it is integral for many applications.

In addition to microfluidics, nanofluidics has also provided an attractive field for various fundamental and practical research studies. Nanofluidics is the study and application of fluids in and around geometries exhibiting nanoscale characteristic dimensions. Nanofluidics is clearly not just an extension of microfluidics, as some have postulated. It has been reported that new physical phenomena and mechanisms that are not observed at microscales or in bulk begin to emerge and dominate at nanoscales. Typical phenomena possessing these characteristics include, nonlinear transport (such as concentration polarization [41-43], ion current rectification [44-46]) and unique liquid properties of water (such as lower dielectric constant [47, 48], higher viscosity [47, 48], and higher proton mobility than in the bulk [49, 50]). These phenomena mostly result from extremely high surface to volume ratios and surface charge exhibited in nanofluidic channels. By using nanospace-specific phenomenon and the advantages described above, many biomolecular applications have been developed in recent years. Recent studies of nanofluidics have demonstrated manipulation of biomolecules (DNA stretching or biomolecule operation by nanostructure-based fluid control) [51-54], biomolecular concentration of DNA or proteins [55-57], separation of DNA or proteins [57-70], and biomolecular interaction analysis [71].

1.3 Separation Analysis of Biomolecules and Miniaturization of Separation Systems

Separation analysis of biomolecules (DNA, RNA, proteins and amino acids) is important in various fields such as fundamental biology and medical diagnosis [72-76]. Separation is often performed prior to analysis of biomolecules. The separation of biomolecules is primarily accomplished using electrophoresis. Agarose gel electrophoresis has been commonly used for the separation of biomolecules; however, there are limitations in terms of separation ability, time constraints, and the requirement for large sample volumes. Miniaturization of separation systems has been achieved thorough capillary electrophoresis and microchip electrophoresis [76-79]. These processes provide a means to achieve high performance and rapid analysis with a reduced cost. It is difficult, however, to integrate additional analysis steps and separation analysis on a single device, as these steps require macromolecules as a separation medium. Recently, research to replace artificial nanostructures with separation media, instead of natural macromolecules, has attracted a great deal of attention [57-70]. Using this technique, high resolution separation has been achieved, and it is clear that there is a unique separation mechanism underlying separation using nanostructures. These nanofluidic-based separation analyses are currently being incorporated into integrated bioanalysis systems.

1.4 Label-Free Detection of Biomolecules

As described in the previous section, tremendous progress has been achieved in development of micro- and nanofluidic technologies for biochemical manipulation. In such miniaturized devices, a more sensitive method for detection is required, as the detection volume is also miniaturized. Detection technologies have also undergone tremendous innovative developments in recent years. In 1959, serum insulin was first analyzed by radioactive element labeling. In the late 1970s, radioactive elements were replaced by enzymes or fluorescent dyes. Following the advent of these initial techniques, various labeling technologies have been developed including fluorescent labeling, isotopic labeling, chemo-luminescent labeling, electrochemically active probe labeling, and nanoparticle labeling [80]. Given that these labeling detection methods are highly sensitive, they are widely used in miniaturized devices. Additionally, at the levels of nanofluidics, fluid control is extremely delicate and it is necessary to monitor this property using a highly sensitive label detection method during operation and at the exit of the nanofluidic channels. The labeling process, however, is complicated and time consuming, thus making this required monitoring difficult. Additionally, the labeling process may alter certain characteristics of samples. First, it is conceivable that charges and sizes can be altered by labeling [81-85]. This may affect molecular dynamics and interaction. It has been reported that the amount of adsorption on the substrate material change due to such changes [86]. It is also believed that labeling agents can interfere with the monitoring of intermolecular interaction by directly binding to biomolecules [80]. This reportedly can lead to underestimation of the interaction between protein and DNA. To solve these problems, researchers must develop a highly sensitive detection method that does not include the process of labeling.

Various label-free detection methods have been reported. These methods include surface plasmon resonance imaging [87-89], the microcantilever method [90-92], the electrochemical method using electrolytic effect transistors [93-95], the electrochemical impedance method [96-

98], the surface enhanced Raman spectroscopy [99-101], and rotating magnetic field analysis [102-104]. These methods are complicated, as it is necessary to modify the receptor on the surface of the detection point, and it is difficult to apply these methods to the monitoring of the flow area. As a method that does not require immobilization, thermal lens microscopy has also been reported; however, this method requires a complicated optical system [105]. The development of a novel label-free detection system that overcomes these problems is desired.

As a simple label-free detection method, a refractometer should be mentioned as a commercially available detector. Figure 1 shows a schematic illustration of the sensor portion of commercially available refractometer. Samples are added drop-wise onto the surface of the sensor and changes in refracted light resulting from the presence or absence of the sample are detected; however, the sensitivity of refractometers is insufficient for application to miniaturized devices. In general, the detection of diffracted light, which is a superposition of waves and possesses a large amount of information, is said to be more sensitive than the detection of refracted light. Figure 2 shows a conceptual illustration of the sensor portion of a diffraction-based refractometer. By introducing a sample into the diffraction grating and detecting the diffracted light, highly sensitive label-free detection can be achieved. In this study, the author aimed to construct a label-free detection system using diffracted light that is compatible with micro- and nanofluidics.

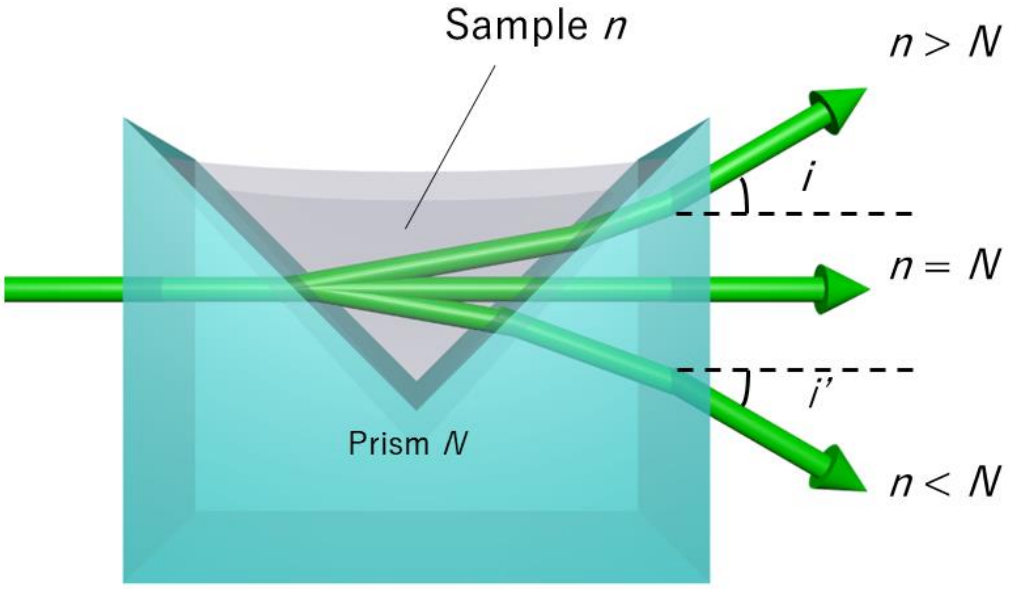

Figure 1. Schematic illustration of the sensor portion of a refractive light detector

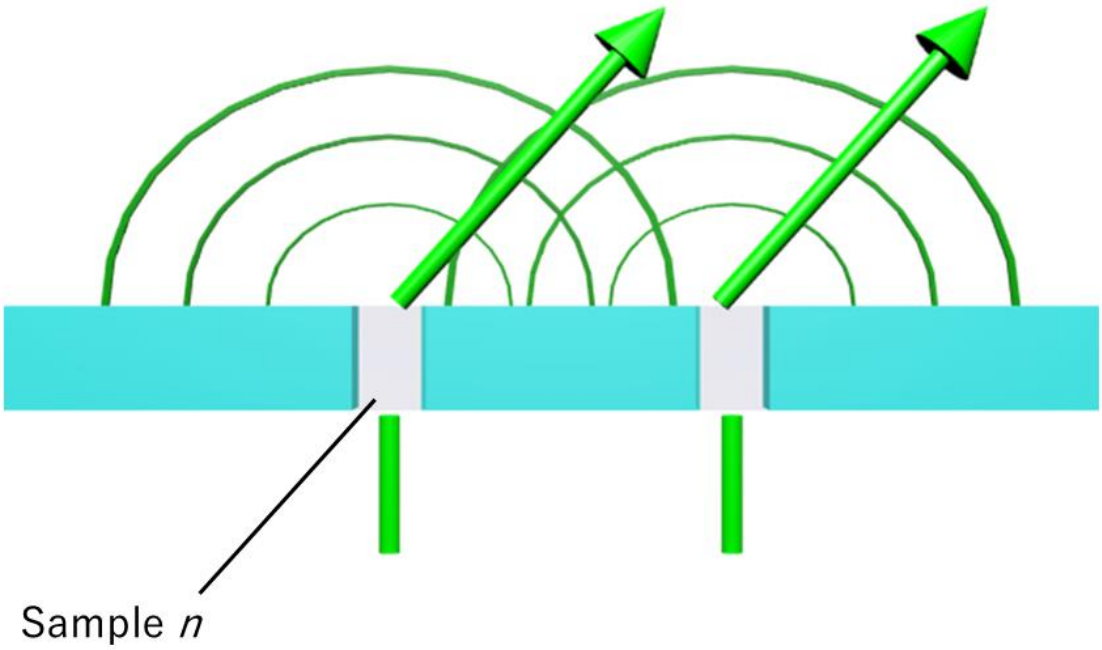

Figure 2. Schematic illustration of the sensor portion of a diffractive light detector

1.4 References

1. T. Van Helvoort, *History of Science* 32.2, 185-235 (1994).
2. X. Fan, I. M. White, S. I. Shopoua, H. Zhu, J. D. Suter, Y. Sun, *Anal. Chim. Acta*, **620**, 8-26 (2008).
3. B. Liu, G. C. Bazan, *Chem. Mater.*, **16**, 4467-4476 (2004).
4. L. M. Smith, J. Z. Sanders, R. J. Kaiser, P. Hughes, C. Dodd, C. R. Connell, C. Heiner, S. B. Kent, L. E. Hood, *Nature*, **321**, 674−679 (1986).
5. F. S. Collins, A. Patrinos, E. Jordan, A. Chakravarti, R. Gesteland, L. Walters, *Science*, **282**, 682-689 (1998).
6. Y. C. Cao,R. Jin, C. A. Mirkin, *Science*, **297**, 1536−1540 (2002).
7. M. Nilsson, H. Malmgren, M. Samiotaki, M. Kwiatkowski, B. C. Chowdhary, U. Landegren, *Science*, **265**, 2085-2088 (1994).
8. C. Larsson, I. Grundberg, O. Söderberg, M. Nilsson, *Nat. Methods*, **7**, 395– 397 (2010).
9. M. Takahashi, K. Nokihara, H. Mihara, *Chem. Biol.*, **10**, 53−60 (2003).
10. P.G. Alluri, M.M. Reddy, K. Bacchawat-Sikder, H.J. Olivos, T. Kodadek, *J. Am. Chem. Soc. 125* (**46**), 13995-14004 (2003).
11. B. H. Jun, H. Kang, Y. S. Lee, D. H. Jeong, *Molecules*, **17**, 2474– 2490 (2012).
12. B. Schweitzer, S. Wiltshire, J. Lambert, S. O'Malley, K. Kukanskis, Z. Zhu, S. F. Kingsmore, P. M. Lizardi, D. C. Ward, Proc. Natl. Acad. Sci., **97**, 10113-10119 (2000).
13. T. J. Polascik, J. E. Oesterling, A. W. Partin, *J. Urol.*, **162**, 293−306 (1999).
14. A. A. Luderer, Y. T. Chen, T. F. Soriano, W. J. Kramp, G. Carlson, C. Cuny, T. Sharp, W. Smith, J. Petteway, M. K. Brawer, *Urology*, *46*, 187−94 (1995).
15. W. J. Catalona, D. S. Smith, R. L. Wolfert, T. J. Wang, H.G. Rittenhouse, T. L. Ratliff, R. B. Nadler, *JAMA, J. Am. Med. Assoc.*, *274*, 1214−20 (1995).
16. A. A. Zachary, *Transplantation*, **86**, 768 (2008).

17. A. Zeevi, A. Girnita, R. Duquesnoy, *Immunol Res*, **36**, 255-264 (2006).
18. N. H. Waseem, D. P. Lane, *J. Cell Sci.* **96**, 121–129 (1990).
19. C. P. Lai, X. O. Breakefield, *Physiol*., **3**, 228 (2012).
20. G. Raposo,W. Stoorvogel, *J. Cell Biol.*, **200**, 373-383 (2013).
21. H. Peinado, M. Alečković, S. Lavotshkin, I. Matei, B. Costa-Silva, G. Moreno-Bueno, M. Hergueta-Redondo, C. Williams, G. García-Santos, C. M. Ghajar, A. Nitadori-Hoshino, C. Hoffman, K. Badal, B. A. Garcia, M. K. Callahan, J. Yuan, V. R. Martins, J. Skog, R. N. Kaplan, M. S. Brady, J. D. Wolchol, P. B. Chapman, Y. Kangm J. Bromberg, D. Lyden, *Nat. Med.*, **18**, 883-891 (2012).
22. J. L. Hood, R. S. San, S. A. Wickline, *Cancer Res.*, **71**, 3792-3801 (2011).
23. D. S. Lincoln, *nature*, **431**, 915-916 (2004).
24. M. Kubo, J. Hata, T. Ninomiya, K. Matsuda, K. Yonemoto, T. Nakano, T. Matsushita, K. Yamazaki, Y. Ohnishi, S. Saito, T. Kitazono, S. Ibayashi, K. Sueishi, M. Iida, Y. Nakamura, Y. Kiyohara., *Nature Genetics*, **39**, 212-217 (2007).
25. D. Miki, M. Kubo, A. Takahashi, KA. Yoon, J. Kim, GK. Lee, JI. Zo, JS. Lee, N. Hosono, T. Morizono, T. Tsunoda, N. Kamatani, K. Chayama, T. Takahashi, J. Inazawa, Y. Nakamura, Y. Daigo, *Nature Genetics*, **42**, 893–896 (2010).
26. Life Technologies Corporation, *JAMA*, **16**, 1629-1631 (2012).
27. B. Q. Xu, N. J. Tao, *Science*, **301**, 1221-1223 (2003).
28. D. Kruger, H. Fuchs, R. Rousseau, D. Marx, M. Parrinello, *Phys. Rev. Lett.*, **89**, 186402 (2002).
29. J. Reichert, R. Ochs, D. Beckmann, H. B. Weber, M. Mayor, H. Lohneysen, *Phys. Rev. Lett.*, **88**, 176804 (2002).
30. S. Nie, S. R. Emory, *Science*, **275** (5303), 1102−1106 (1997).
31. A. Manz, N. grabber, H. Widmer, *Sensors and Actuators B: Chemical*, **1**, 244-248 (1990).
32. D. R. Reyes, D. Iossifidis, P. A. Auroux, A. Manz, *Anal. Chem.*, 2002, **74**, 2623-2636 (2002).

33. P.A. Auroux, D. Iossifidis, D.R. Reyes, A. Manz, *Anal. Chem.* 2002, **74**, 2637-2652 (2002).

34. T. Vilkner, D. Janasek, A. Manz, *Anal. Chem.*, **76**, 3373-3386 (2004).

35. P. S. Dittrich, K. Tachikawa, A. Manz, *Anal. Chem.*, **78**, 3887-3907 (2006).

36. G. M. Whitesides, *Nature*, **442**, 368-373 (2006).

37. D. Janasek, J. Franzke, A. Manz, *Nature*, **442**, 374-380 (2006).

38. D. Psaltis, S. R. Quake, C.H. Yang, *Nature*, **442**, 381-386 (2006)

39. H. Craighead, *Nature*, **442**, 387-393 (2006).

40. A. J. deMello, *Nature*, **442**, 394-402 (2006).

41. L. Cao, F. Xiao, Y. Feng, W. Zhu, W. Geng, J. Yang, X. Zhang, N. Li, W. Guo, L. Jiang, *Adv. Funct. Mater.*, **27**, 1604302 (2017).

42. A. Syed, L. Mangano, P. Mao, J. Han, Y.-A. Song, K. Liu, Z.-Y. Wu, Y. Fouillet, *Lab Chip*, **14**, 4455 (2014).

43. A.C. Louër, A. Plecis, A. Pallandre, J. C. Galas, A. Estevez-Torres, A. M. Haghiri-Gosnet, *Anal. Chem*., **85**, 7948-7956 (2013).

44. H. Zhang, Y. Tian, L. Jiang, *Nano Today*, **11**, 61-81 (2016).

45. T. Gamble, K. Decker, T. S. Plett, M. Pevarnik, J.-F. Pietschmann, I. Vlassiouk, A. Aksimentiev, Z. S. Siwy, *J. Phys. Chem. C*., **118**, 9809-9819 (2014).

46. M. Zhang, X. Hou, J. Wang, Y. Tian, X. Fan, J. Zhai, L. Jiang, *Adv. Mater.*, **24**, 2424 (2012).

47. Y. Xu, B. Xu, *Small*, **11**, 6165-6171 (2015).

48. A. Hibara, T. Saito, H.-B. Kim, M. Tokeshi, T. Ooi, M. Nakao, T. Kitamori, *Anal. Chem.*, **74**, 6170-6176 (2002).

49. H. Chinen, K. Mawatari, Y. Pihosh, K. Morikawa, Y. Kazoe, T. Tsukahara, T. Kitamori, *Angew. Chem., Int. Ed.*, **51**, 3573-3577 (2012).

50. T. Tsukahara, A. Hibara, Y. Ikeda, T. Kitamori, *Angew. Chem., Int. Ed.*, **46**, 1180-1183 (2007).

51. D. Huh, K. L. Mills, X. Zhu,M. A. Burns, M. D. Thouless, S. Takayama, Nat. Mater., **6**,

424−428 (2007**)**.

52. C. Wang, S. W. Nam, J. M. Cotte, C. V. Jahnes, E.G. Colgan, R. L. Bruce, M. Brink, M. F. Lofaro, J. V. Patel, L. M. Gignac, E. A. Joseph, S. P. Rao, G. Stolovitzky, S. Polonsky, Q. Lin, *Nat. Commun.*, **8**, 14243 (2017).
53. Y. Xu, *Adv. Mater.*, **30**, 1870019 (2018).
54. Amin, S.; Khorshid, A.; Zeng, L.; Zimny, P.; Reisner, W. *Nat. Commun.*, **9**, 1506 (2018).
55. Wang, Y. C.; Stevens, A. L.; Han, J. *Anal. Chem.*, **77**, 4293-4299 (2005).
56. D. Stein, Z. Deurvorst, F. H. van der Heyden, W. J. Koopmans, A. Gabel, C. Dekker, *Nano Lett.*, **10**, 765-772 (2010).
57. S. H. Ko, D. Chandra, W. Ouyang, T. Kwon, P. Karande, J. Han, Nat. Nanotechnol., **12**, 804-812 (2017).
58. J. Han, S. W. Turner, H. G. Craighead, *Phys. Rev. Lett.*, **83**, 1688−1691 (1999).
59. J. Han, H. G. Craighead, *Science*, **288**, 1026-1029 (2000).
60. N. Kaji, Y. Tezuka, Y. Takamura, M. Ueda, T. Nishimoto, H. Nakanishi, Y. Horiike, Y. Baba, *Anal. Chem.*, **76**, 15−22 (2004).
61. J. Fu, J. Yoo, J. Han, *Phys. Rev. Lett.*, **97**, 018103 (2006)
62. J. Fu, R. B. Schoch, A. L. Stevens, S. R. Tannenbaum, J. Han, *Nat. Nanotechnol*., **2**, 121-128 (2007).
63. N. Laachi, C. Declet, C. Matson, K. D. Dorfman, *Phys. Rev. Lett.*, **98**, 098106 (2007).
64. T. Yasui, N. Kaji, M. R. Mohamadi, Y. Okamoto, M. Tokeshi, Y. Horiike, Y. Baba, *ACS Nano*, **5**, 7775-7780 (2011).
65. Yasui, T.; Kaji, N.; Ogawa, R.; Hashioka, S.; Tokeshi, M.; Horiike, Y.; Baba, Y. Anal. Chem., **83**, 6635-6640 (2011).
66. S. G. Park, D. W. Olson, K. D. Dorfman, *Lab Chip*, **12**, 1463-1470 (2012).

67. T. Yasui, N. Kaji, Y. Okamoto, M. Tokeshi, Y. Horiike, Y. Baba, *Microfluid. Nanofluid.*, **14**, 961-967 (2013).

68. T. Yasui, S. Rahong, K. Motoyama, T. Yanagida, Q. Wu, N. Kaji, M. Kanai, K. Doi, K. Nagashima, M. Tokeshi, M. Taniguchi, S. Kawano, T. Kawai, Y. Baba, *ACS Nano*, **7**, 3029-3035 (2013).

69. S. Rahong, T. Yasui, T. Yanagida, K. Nagashima, M. Kanai, A. Klamchuen, G. Meng, Y. He, F. Zhuge, N. Kaji, T. Kawai, Y. Baba, *Sci. Rep.*, **4**, 5252-5259 (2014).

70. T. Yasui, N. Kaji, R. Ogawa, S. Hashioka, M. Tokeshi, Y. Horiike, Y. Baba, *Nano. Lett.*, **15**, 3445-3451 (2015).

71. F. Liang, Y. Guo, S. Hou, Q. Quan, *Sci. Adv.*, **3**, e1602991 (2017).

72. M. Orita, H. Iwahana, H. Kanazawa, K. Hayashi, T. Sekiya, *PNAS*. **86**, 2766−2770 (1989).

73. M. R. Shortreed, H. Li, W. H. Huang, E. S. Yeung, *Anal. Chem.*, **72**, 2879–2885 (2000).

74. M. S. Rashed, P. T. Ozand, M. P. Bucknall, D. Little, *Pediatr. Res.*, **38**, 324−31 (1995).

75. M. Unlu, M. E. Morgan, J. S. Minden, *Electrophoresis*, **18**, 2071−2077 (1997).

76. Z. D. Sandlin, M. Shou, J. G. Shackman, R. T. Kennedy, *Anal. Chem.*, **77**, 7702−7708 (2005).

77. W. N. Vreeland, R. J. Meagher, A. E. Barron, Anal. Chem., **74**, 4328–4333 (2002).

78. Y. W. Lin, M. J. Huang, H. T. Chang, *J. Chromatogr. A*, **1014**, 47–55 (2003).

79. L. Wang, J. Wu, Q. Wang, C. He, L. Zhou, J. Wang, Q. Pu, *J. Agric. Food Chem*., **60**, 1613–1618 (2012).

80. A. Syahir, K. Usui, K.Y. Tomizaki, K. Kajikawa, H. Mihara, *Microarrays*, **4** (2), 228-244 (2015).

81. B. Kundukad, J. Yan, P. S. Doyle, *Soft Matter*, **10**, 9721-9728 (2014).

82. C. Carlsson, A. Larsson, M. Jonsson, *Electrophoresis*, **17**, 642-651 (1996**)**.

83. M. Eriksson, M. Mehmedovic, G. Westman, B. Akerman, *Electrophoresis*, 26, 524-532 (2005).

84. F. Dang, W. Li, L. Zhang, J. Mohammad, I. Tatsuhiro, H. Kiwada, N. Kaji, T. Manabu, Y. Baba,. *J. Chromatogr. A*, **1118**, 218–225 (2006).

85. S. Quake, H. Babcock, S. Chu, *Nature*, **388**, 151-154 (1997).

86. J. Romanowska, D. B. Kokh, R. C. Wade, *Nano Lett.*, **15**, 7508-7513 (2015).

87. M. A. Cooper, *Nat Rev Drug Discov*, **1**, 515-528 (2002).

88. S. Hana, Z. Shile, M. D. Aimee, G. David, W. Kai, H. Jiri., *Anal. Chem.,* **82,** 10110–10115 (2010).

89. M. Piliarik, M. Vala, I. Tichy, J. Homola., *Biosens. Bioelectron.,* **24**, 3430-3435 (2009).

90. G. Shekhawat, S. H. Tark,V. P. Dravid, *Science,* **311**, 1592-1595 (2006).

91. R. Raiteri, M. Grattarola, H. J. Butt, P. Skladal, *Sens. Actuators B,* **79**, 115-122 (2005).

92. G. Wu, H. Ji, K. Hansen, T. Thundat, R. Datar, R. Cote, M. F. Hagan, A. K. Charkraborty, A. Majumdar, *PNAS.*, **98**, 1560-1564 (2001).

93. J. Chaste, A. Eichler1, J.Moser, G. Ceballos, R. Rurali, A. Bachtold, *Nat. nanotech.,* **7,** 301-304 (2012).

94. Y. T. Yang, C. Callegari, X. L. Feng, M. L. Roukes, *Nano Lett*., **11,** 1753-1759 (2011).

95. A. N. Cleland, *New J. Phys*., **7**, 235 (2005).

96. M. Giovanni, A. Bonanni, M. Pumera, *Analyst*, **24**, 580-583 (2012).

97. E. Katz, I. Willner, *Electroanalysis*, **15**, 913-947 (2003).

98. C. X. Lim, H. Y. Hoh, P. K. Ang, K. P. Loh, *Anal. Chem.*, **82**, 7387–7393 (2010).

99. I. Choi, Y. S. Huh, D. Erickson, *Lab Chip,* **11,** 632–638 (2011).

100. S. M. Park, Y. S. Huhb, H. G. Craigheada, D. Erickson, *PNAS* , **37**, 15549–15554 (2009).

101. Inhee. Choi, Yun Suk Huh, and David Erickson: *The proceedings of μTAS 2011*, **20**, 476-478 (2011).

102. D. C. Leslie, J. Li, B. C. Strachan, M. R. Begley, D. Finkler, L. A. L. Bazydlo, N. C. Barker, D. M. Haverstick, M. Utz, J. P. Landers, *J. Am. Chem. Soc.*, 134 (**12**), 5689–5696 (2012).

103. N. Osterman, I. Poberaj, J. Dobnikar, D. Frenkel, P. Ziherl, D. Babic, *Phys. Rev. Lett.*, **103**, 228301 (2009).

104. A. Ahniyaz, Y. Sakamoto, L. Bergström, *PNAS.*, **104**, 17570-17574 (2007).

105. M. Tokeshi, M. Uchida, A. Hibara, T. Sawada, T. Kitamori, *Anal. Chem.*, **73**, 2112−2116 (2001).

Chapter 2.
Fabrication of
Micro- and Nanofluidic Devices

2.1 Introduction

Nanometer range channels have attracted attention for use in both fundamental studies [1-10] and application-based technologies [11-20] as they have unique and useful applications in biomolecular manipulation and control. Despite a wide range of applications, nanofluidics are not as widely used for practical applications compared to microfluidics. One critical issue underlying nanofluidics is the fabrication of nanofluidic channels. Although it is possible to partially fabricate nanofluidic channels using high-precision UV lithography processing technology [21, 22], it is still difficult to apply general UV lithography to fabricate nanometer-range channels due to the diffraction limit.

Electron beam lithography is the practice of focusing a beam of electrons to draw custom shapes on electron-sensitive resistors. The electron beam changes the solubility of the resistor, enabling selective removal of either the exposed (positive) or non-exposed (negative) regions of the resistor. This technique has been widely used for patterning nanofluidic channels, as it allows for the creation of extremely small patterns that are difficult to produce with general photolithography techniques [4, 7-10, 12-15, 17-20]. This technique can pattern various structures due to its design flexibility, however, it is time consuming and requires expensive and dedicated facilities.

Laser interference lithography (LIL) is a patterning technique that does not require dedicated facilities or photomasking [23-26]. Two split laser beams are directed by mirrors and superimposed on the photoresist material. Thus, the photoresist material is exposed via the interference pattern. Conventional electron beam lithography techniques are delicate and expensive and require highly skilled operators and/or large budgets to maintain the system. Additionally, the patterning of large areas is time consuming. Although laser interference lithography can only pattern repeated structures, it possesses advantages such as high-throughput, low cost, and large pattern area (meter-scale) capabilities.

In this section, nanochannels were patterned using two methods. One used electron beam lithography, and the other used laser interference lithography. Patterned nanochannels were connected to a microchannel patterned by photolithography. Additionally, pressure-driven devices and electric field driven devices were both fabricated, as introduction of a sample solution occurs in nanofluidic channels possessing a small channel volume.

2.2 Experimental Design

2.2.1 Electron Beam Lithography

Figure 3 shows a schematic illustration of the device fabrication processes. The device was designed to facilitate solution flow via pressure. Microchannels and nanochannels were separately fabricated on a fused silica substrate (76.4 mm × 25.4 mm). General photolithography techniques and plasma etching were used for microchannel fabrication. After spin-coated (2000 rpm, 60s) silane coupling agent (OAP) and positive photo resistor exposure (OFPR-800), microchannels (width, 200 μm) were patterned by exposing to UV light through a photomask and then developing. For nanochannel fabrication, electron beam lithography techniques and dry etching were used. High resolution positive electron beam resistors and conductive polymers were spin-coated on the fused silica substrate. Nanowall channels (width, 300 nm; gap, 600 nm; length, 1.2 mm) were patterned by an electron beam lithography system at the center of the substrate. Both fabricated channels were dry etched (depth, microchannel; 2 μm, nanochannel; 250 nm), and inlet holes and outlet holes were drilled into the microchannels by a diamond-coated drill. The author fabricated the micro- and nanofluidic devices by bonding these two substrates by thermal fusion bonding during an alignment step.

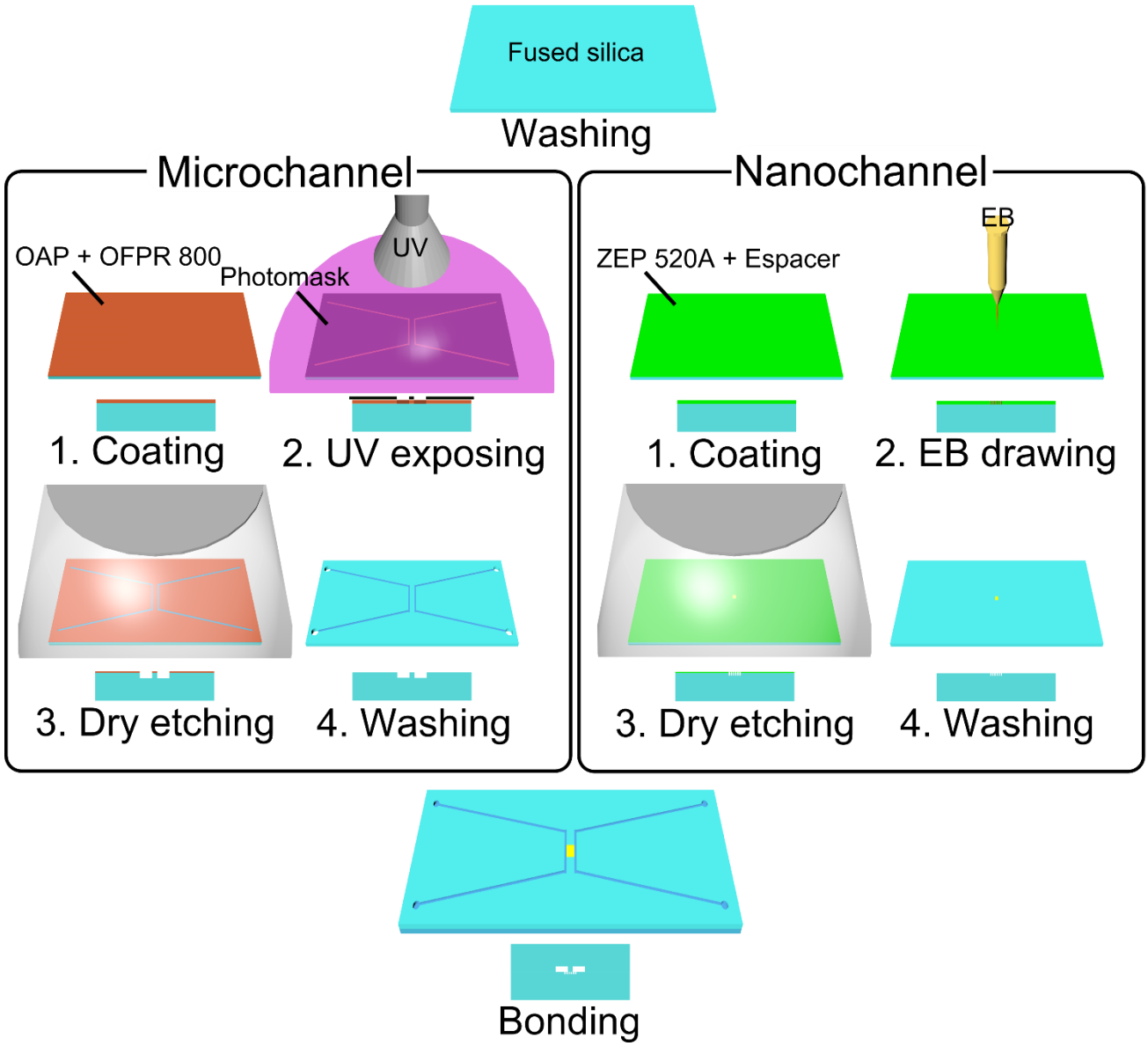

Figure 3. Schematic illustration of micro- and nanofluidic device fabrication based on EB lithography. The upper shows a schematic view and the lower shows a cross-section of each step.

2.2.2 Laser Interference Lithography

Here, the author designed two types of devices using laser interference lithography techniques. One is nanowall device with linear nanochannels periodically arranged into a microchannel. The other is nanopillar device consisting of cylinder shaped structures (nanopillar) periodically arranged into a microchannel.

a. Nanowall device

Figure 4 shows a schematic illustration of the nanowall device fabrication processes. First, the cross-shaped microchannel (width, 50 μm) was patterned in a manner similar to the conventional photolithography method. After spin-coating with an adherence agent (AZ AD promotor) and photoresistor (TDMR-AR80) at 2500 rpm for 60 s, the fused silica substrate was pre-baked at 95°C for 20 min, and then the anti-reflection reagent (AZ Aquatar) was spin-coated onto the top surface. The coated substrate was exposed to UV light through a photomask. This photomask was designed to seal a portion of the cross-shaped microchannel, and the nanochannels were patterned around this closed portion using laser interference lithography after microchannel patterning. Figure 5 shows a schematic illustration of the experimental setup for laser interference lithography. A collimated light beam from a He-Cd laser (325 nm in wavelength; Model IK3401R-F; Kimmon Electric Company, Ltd., Tokyo) was separated into ±1st order diffracted beams using a phase mask (Ibsen Photonics A/S) and then interfered onto the sample stage. We set the incident angle to allow the fringe pitch to reach 900 nm, as calculated from Bragg's law. The interference beam was illuminated at the center of the substrate (ϕ5 mm area) for 70 s. After baking for 90 s at 110°C, the photoresistor was developed and rinsed in the developer for 90 s and then in water for 10 s. The patterned substrate was etched in a gas mixture consisting of CHF_3 (5 cc/min) and Ar (20 cc/min) using an ICP dry etcher (ICP power, 50 W; bias power, 25 W; substrate

temperature, 25°C) (RIE-101iP, Samco Inc., Kyoto). Finally, the micro- and nano-patterned substrate was bonded to another fused-silica substrate, which had inlet and outlet holes drilled with a diamond-coated drill by thermal fusion bonding (1080°C, under vacuum). The bonding process did not affect the structural integrity of the nanochannels.

b. Nanopillar device

Figure 6 shows a schematic illustration of the nanopillar device fabrication process. Here, the nanopillars were fabricated only within the microchannel (width, 50 μm). Cr was sputtered onto the cleaned fused silica substrate, and then a silane coupling agent (OAP), photoresist (OFPR-5000), was spin-coated sequentially. Exposure was carried out using a photomask, and the microchannels were patterned after development (NMD-3) and Cr etching (Cr etchant). Subsequently, patterning of nanopillar structures was performed. The photoresist used above was removed by washing with acetone, and an adherence agent (AZ AD promotor), photoresist (TDMR-AR80), and an antireflective agent (Aquatar) were spin-coated on the substrate sequentially. Two-dimensional laser interference lithography was used to pattern the nanopillar. Following laser interference exposure as described above, the substrate was rotated 90° and a second exposure was conducted. After this, the photoresist in the unwanted component was removed by exposure through a photomask and developing. Subsequently, dry etching was performed to fabricate the substrate with patterned structures. Inlet holes and outlet holes were drilled at the edge of the microchannel using a diamond-coated drill. Finally, the nanopillar device was completed by bonding to another fused silica substrate.

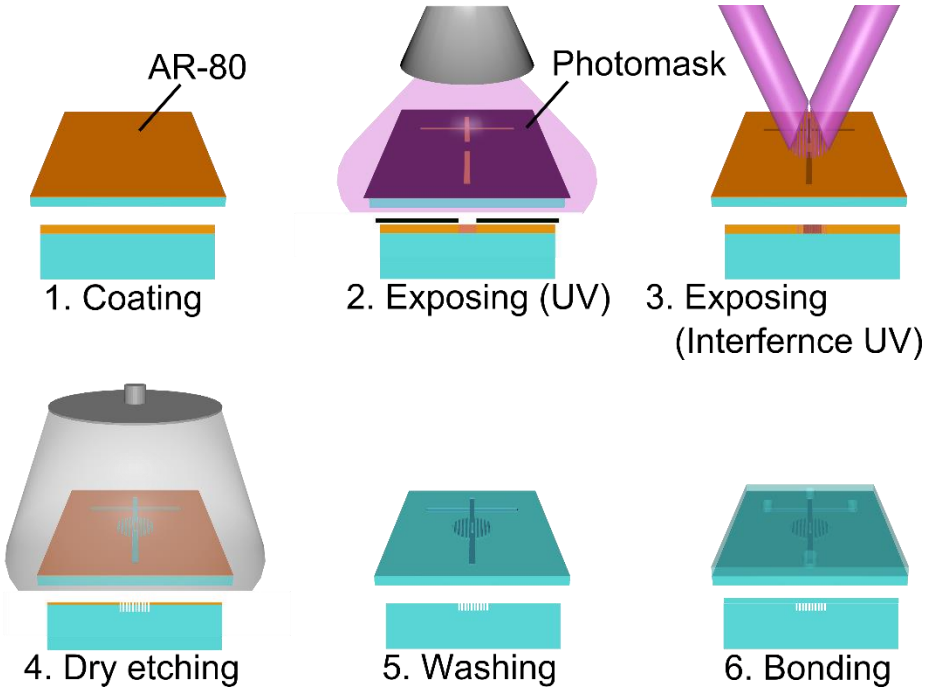

Figure 4. Schematic illustration of nanowall device fabrication based on laser interference lithography. The upper shows a schematic view and the lower shows a cross-section of each step.

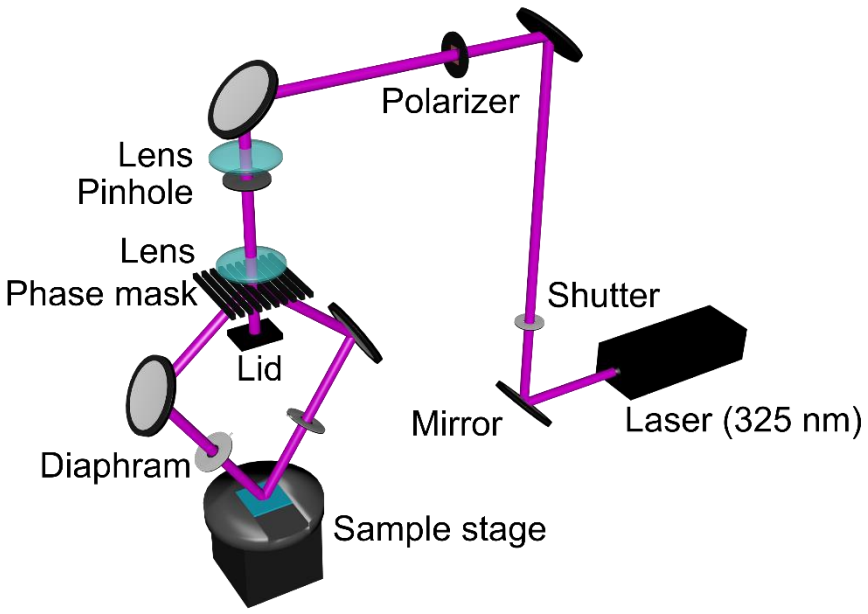

Figure 5. Schematic illustration of the experimental setup for the laser interference lithography.

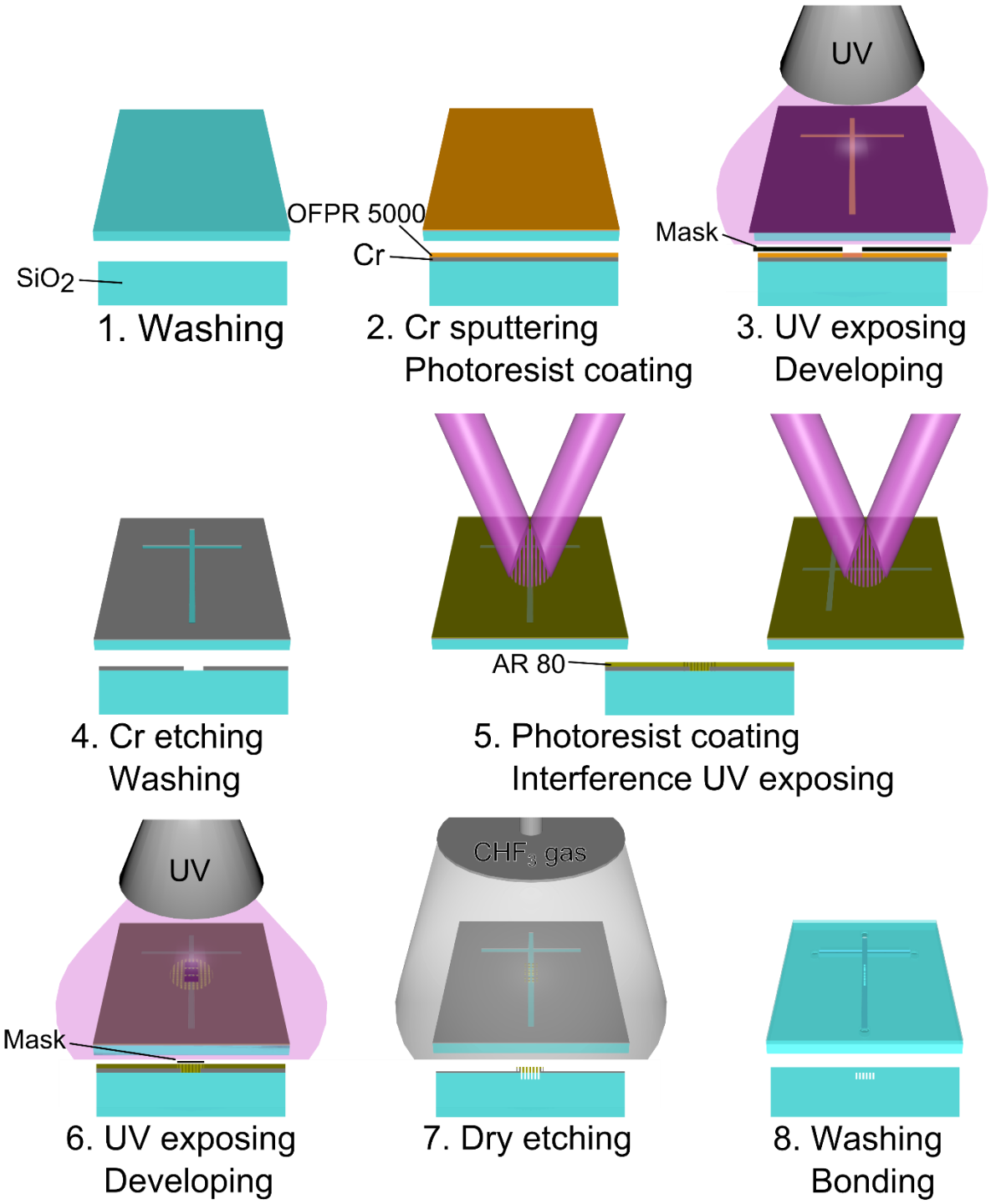

Figure 6. Schematic illustration of nanopillar device fabrication based on laser interference lithography. The upper panel shows a schematic view and the lower panel shows a cross-section of each step.

2.2.4 Chemicals and Reagents

Ultrapure water was obtained using a Direct-Q UV system (Merck Millipore, Tokyo). Fused silica substrates were purchased from Daico MFG Co., Ltd. (Kyoto) (n = 1.460118 at λ = 546.074 nm (from the company's data sheet)) or Shin-Etsu Chemical Co., Ltd. (Tokyo, Japan) (n=1.4610 at λ=530.9 nm (from the company's data sheet)). High resolution positive electron beam resist (ZEP-520-A), developer (ZED-N50), rinse (ZMD-D) and remover (ZDMAC) for fabrication of nanochannels were purchased from Zeon Corporation (Tokyo, Japan). Conductive polymer (Espacer) used for the charge dissipating agent in electron beam lithography was purchased from Showa Denko K.K. (Tokyo, Japan). A positive photo resist (TDMR-AR80) and developer (NMD-3) for fabricating the micro- and nanofluidic device at laser interference lithography were purchased from Tokyo Ohka Kogyo Co., Ltd. (Tokyo). An adherence agent (AZ AD promotor) and an anti-reflection reagent (AZ Aquatar) were purchased from AZ Electronic Materials Co., Ltd. (Tokyo). Silane coupling agent (OAP), positive photo resist (OFPR-800, 5000) and developer (NMD-3) for fabrication of microchannels were purchased from Tokyo Ohka Kogyo Co., Ltd. (Tokyo, Japan). Cr etchant was purchased from KANTO CHEMICAL Co., Inc. (Tokyo).

2.3 Results and Discussion

2.3.1 Evaluation of the device

a. EB lithography based nanowall device

Figure 7 shows an example of the device photo and a SEM image of the nanochannels. The device was designed for pressure-driven flow. Pressure-based regulation of the sample was difficult due to unexpected reductions in pressure. Here, pressure-driven nanofluidic control was achieved by connecting the two open-channel microchannels with the nanochannels. These were easily controlled by the syringe pump connected to the fabricated device. From the SEM image of the nanochannel prior to bonding with the microchannel, it was clear that the fabricated nanochannels were periodically arranged as designed, and the nanofluidic channels were of high quality. The cross sectional view of the channels was achieved by cutting the substrate. Although the dust and debris was observed when the substrate was cut, the clear rectangular structure of the nanochannels was also observed without the taper. Although only simple periodic structures were patterned in this study, this method is useful for lab-based research, as it is possible to pattern various structures with high precision.

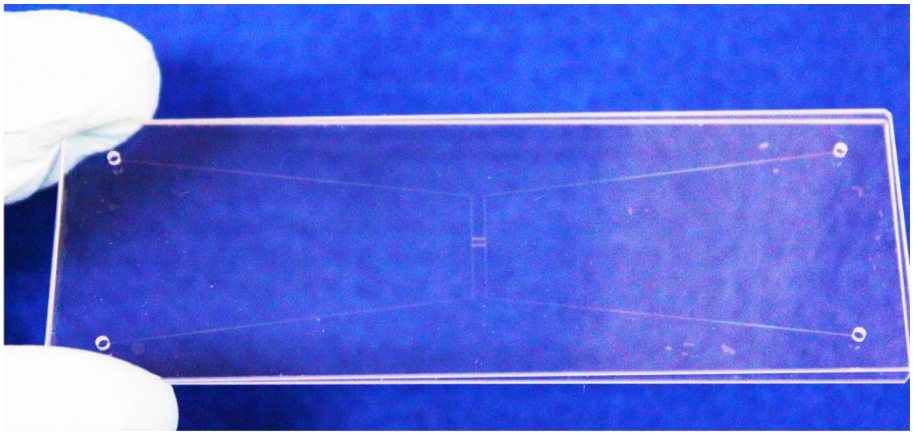

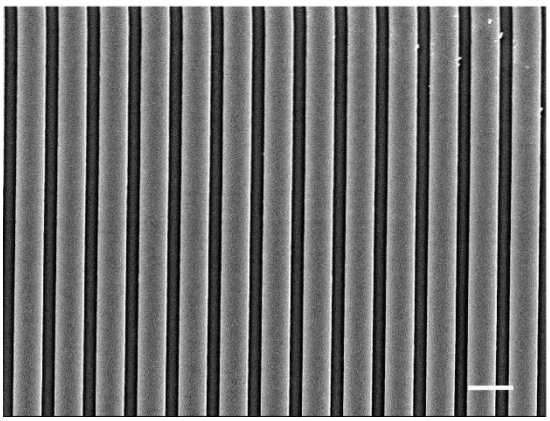

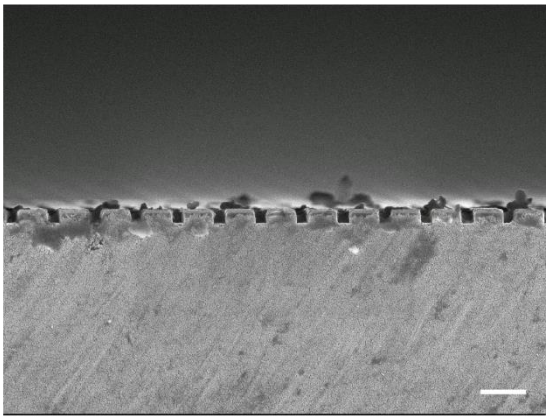

Figure 7. A photo of the micro- and nanofluidic device and SEM images of nanofluidic channels fabricated by the electron beam lithography technique; scale bar, 1 μm.

b. Laser interference lithography based nanowall device

Figure 8 provides an example of the device image and an AFM image of the nanochannels. The device was designed for electric field-driven flow. It is possible to control the sample by either electroosmotic flow or electrophoresis by applying an electric field to the device, as it is composed of fused silica. The AFM image indicates that the periodic nanochannels were successfully fabricated on the fused silica substrate by laser interference lithography. These nanochannels were 500 nm wide, 350 nm deep, and spaced at 400 nm intervals. Fabrication of the nanochannel by electron beam lithography took approximately 20 min to pattern a 1.2-mm square. Additionally, it was difficult to expand the patterning area. Conversely, laser interference lithography can complete patterning in a short time (70 s) and the patterning area can be easily expanded by expanding the laser spot size (meter-scale). Therefore, this method is suited to mass production, as it can pattern multiple substrates simultaneously if the substrate size is sufficiently small.

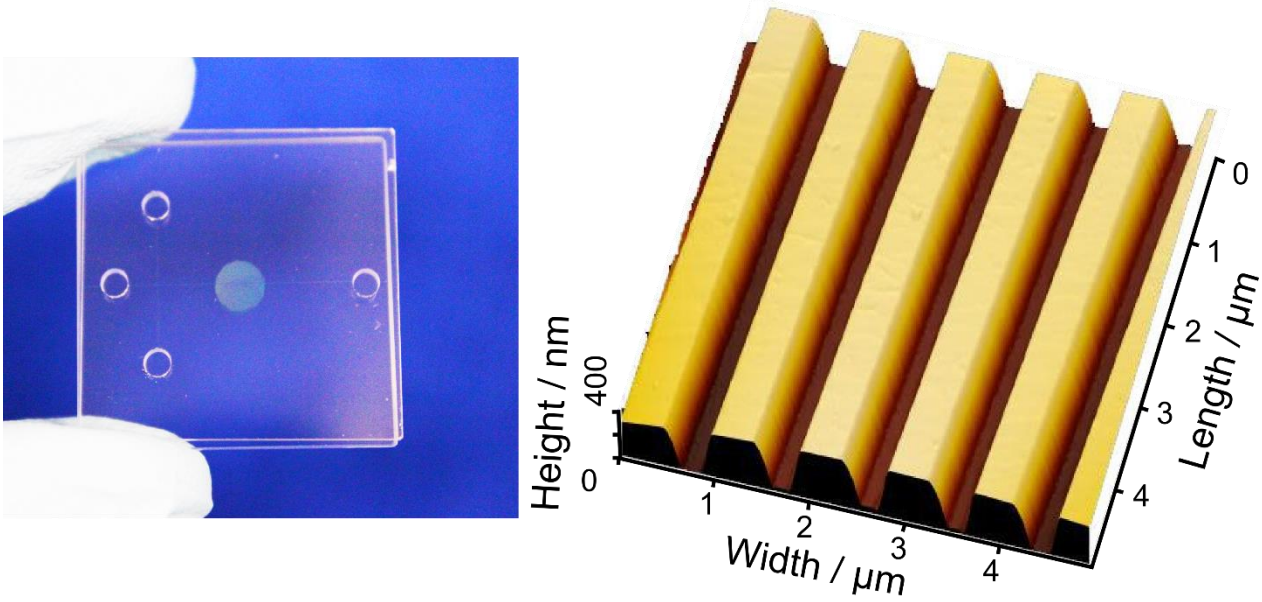

Figure 8. A photo of the micro- and nanofluidic device and AFM images of nanofluidic channels fabricated by the laser interference lithography technique; scale bar, 1 μm.

c. Laser interference lithography-based nanopillar device

To demonstrate the utility of the laser interference lithography technique in the context of nanofluidics, periodically arranged nanopillars were fabricated within a microchannel. Figure 9 shows the image of the device and nanopillar structures. The substrate was exposed in a grid pattern by two dimensional laser interference exposure. After one exposure, the substrate was rotated by 90° and exposed again. At this time, the intersection point of the photoresist is in an overdose state due to the double exposure, resulting in a cylindrical structure. The fabricated nanopillars exhibit fine cylindrical shapes, and they possess a 450 nm diameter, 350 nm height, and are aligned at 450 nm intervals. This demonstrates that the nanopillars can be easily patterned within the microchannel without using electron beam lithography. The angle of nanopillar arrangement within the microchannel can be adjusted by adjusting the angle of the substrate placed on the sample stage during laser interference exposure (Figure 10). Here, the size of the structures is dependent upon the time of laser interference exposure (Figure 11). When the duration of exposure is long, smaller nanopillars are patterned, and in the case of shorter exposures, large nanopillars are patterned. Additionally, when the exposure time is too short, only the intersection point of the double exposure is developed. In this study, dry etching was performed using photoresist as a mask, and it was therefore difficult to pattern high aspect ratio structures. When fabricating a structure with a higher aspect ratio, it is possible to create a mask that is resistant to etching by removing metal from this hole. As described above, this method is useful for patterning a periodic structure due to its ease, rapidity, and low cost compared to that of the method using electron beam lithography.

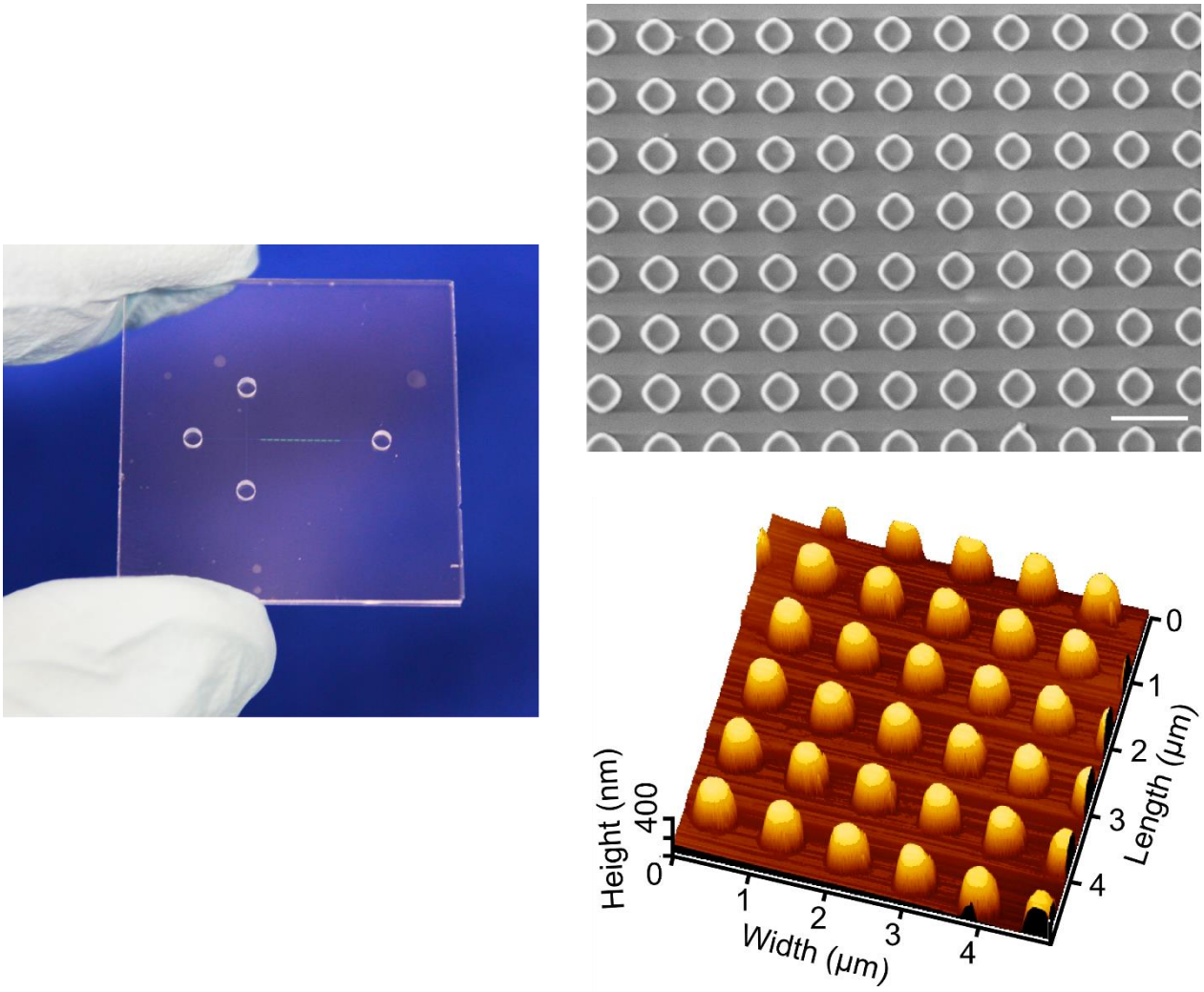

Figure 9. A photo of the micro- and nanofluidic device (nanopillar device) and SEM and AFM images of nanochannels fabricated by the laser interference lithography technique; scale bar, 1 μm.

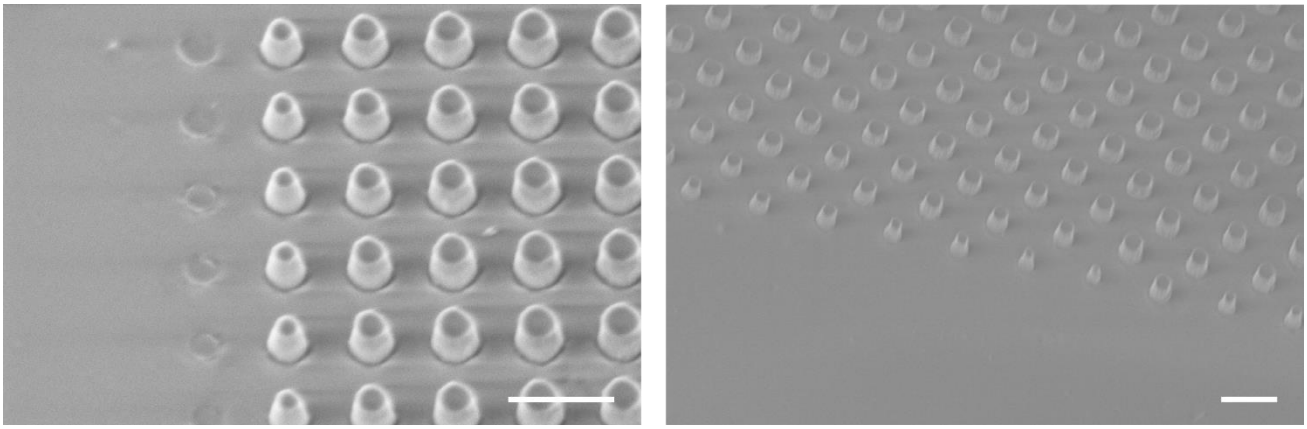

Figure 10. SEM images of the square and tilted patterned nanopillars. scale bar: 1 m

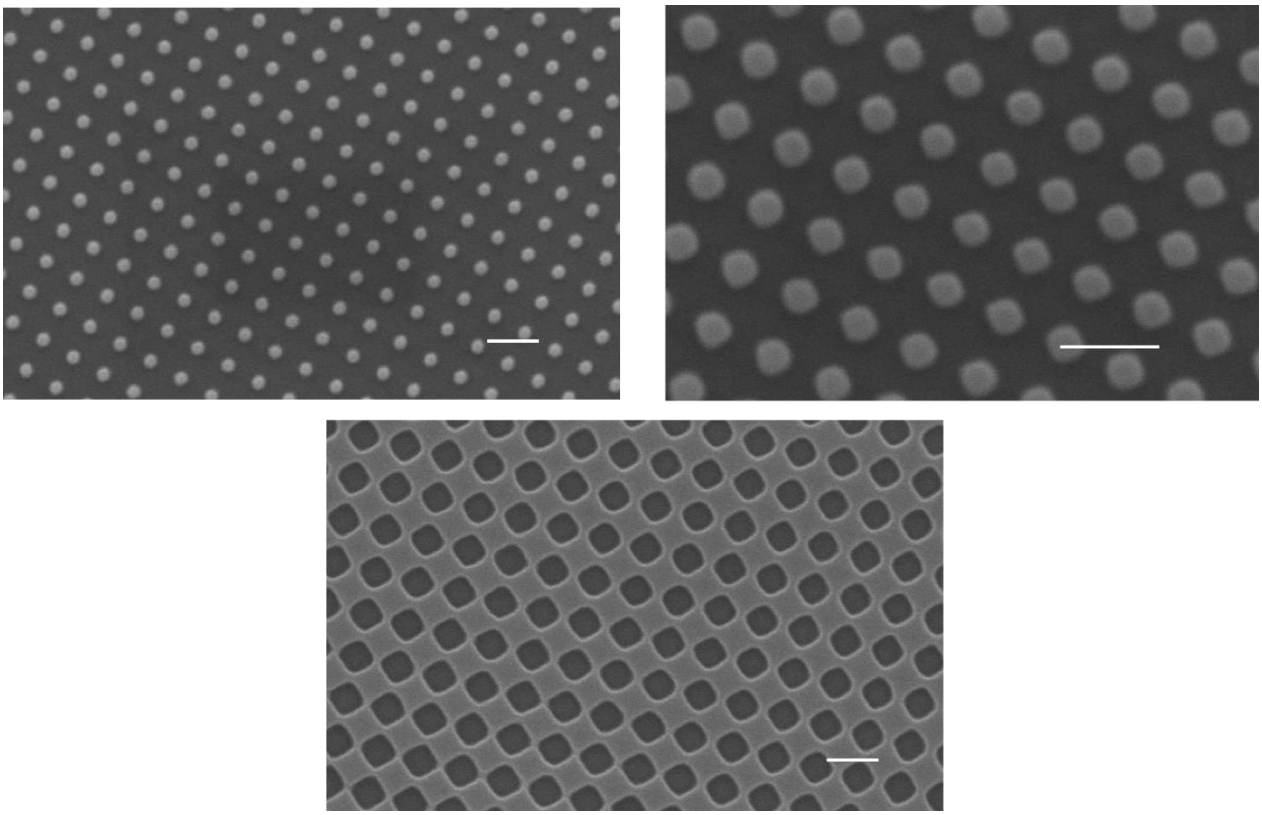

Figure 11. SEM images of the photo resist at various exposure times. Top-left; longer exposure time, top-right; medium exposure time, bottom; too short exposure time. Scale bar: 1 m

2.4 Conclusions

Micro- and nanofluidic devices were fabricated in two ways. First, micro- and nanofluidic devices were fabricated by combining electron beam lithography and photolithography techniques. Microchannels and nanochannels were patterned on two individual substrates, resulting in the suppression of pressure loss that enabled pressure-driven control of the fluid. This fabrication method exhibits flexibility for patterning design and can be applied to various micro- and nanofluidic device fabrications.

Second, a method based on the laser interference lithography technique was also employed. In this study, nanowall devices and nanopillar devices were fabricated by performing one- and two-dimensional laser interference exposures. The nanostructures were able to pattern in an arbitrary area within the microchannel after co-treatment with photolithography techniques. Additionally, it is difficult to expand the patterning area. Conversely, laser interference lithography can complete patterning in a short time (~ 1 min for single exposure), and the patterning area can be easily expanded by expanding the laser spot size. This method is also suited to mass production as it can pattern multiple substrates simultaneously if the substrate size is sufficiently small. Our current findings demonstrate that the combined use of laser interference lithography with conventional photolithography is a useful method for micro- and nanofluidic device fabrication.

2.5 References

1. L. Cao, F. Xiao, Y. Feng, W. Zhu, W. Geng, J. Yang, X. Zhang, N. Li, W. Guo, L. Jiang, *Adv. Funct. Mater.*, **27**, 1604302 (2017).
2. A. Syed, L. Mangano, P. Mao, J. Han, Y. A. Song, K. Liu, Z. Y. Wu, Y. Fouillet, *Lab Chip*, **14**, 4455-4460 (2014).
3. A. C. Louër, A. Plecis, A. Pallandre, J. C. Galas, A. Estevez-Torres, A. M. Haghiri-Gosnet, *Anal. Chem.*, **85**, 7948-7956 (2013).
4. H. Zhang, Y. Tian, L. Jiang, *Nano Today*, **11**, 61-81 (2016).
5. T. Gamble, K. Decker, T. S. Plett, M. Pevarnik, J.-F. Pietschmann, I. Vlassiouk, A. Aksimentiev, Z. S. Siwy, *J. Phys. Chem. C.*, **118**, 9809-9819 (2014).
6. M. Zhang, X. Hou, J. Wang, Y. Tian, X. Fan, J. Zhai, L. Jiang, *Adv. Mater.*, **24**, 2424 (2012).
7. Y. Xu, B. Xu, *Small*, **11**, 6165-6171 (2015).
8. A. Hibara, T. Saito, H.-B. Kim, M. Tokeshi, T. Ooi, M. Nakao, T. Kitamori, *Anal. Chem.*, **74**, 6170-6176 (2002).
9. H. Chinen, K. Mawatari, Y. Pihosh, K. Morikawa, Y. Kazoe, T. Tsukahara, T. Kitamori, *Angew. Chem., Int. Ed.*, **51**, 3573-3577 (2012).
10. T. Tsukahara, A. Hibara, Y. Ikeda, T. Kitamori, *Angew. Chem., Int. Ed.*, **46**, 1180-1183 (2007).
11. D. Huh, K. L. Mills, X. Zhu,M. A. Burns, M. D. Thouless, S. Takayama, Nat. Mater., **6**, 424−428 (2007**)**.
12. C. Wang, S. W. Nam, J. M. Cotte, C. V. Jahnes, E.G. Colgan, R. L. Bruce, M. Brink, M. F. Lofaro, J. V. Patel, L. M. Gignac, E. A. Joseph, S. P. Rao, G. Stolovitzky, S. Polonsky, Q. Lin, *Nat. Commun.*, **8**, 14243 (2017).
13. Y. Xu, *Adv. Mater.*, **30**, 1870019 (2018).
14. Amin, S.; Khorshid, A.; Zeng, L.; Zimny, P.; Reisner, W. *Nat. Commun.*, **9**, 1506 (2018).
15. Wang, Y. C.; Stevens, A. L.; Han, J. *Anal. Chem.*, **77**, 4293-4299 (2005).

16. D. Stein, Z. Deurvorst, F. H. van der Heyden, W. J. Koopmans, A. Gabel, C. Dekker, *Nano Lett.*, **10**, 765-772 (2010).
17. S. H. Ko, D. Chandra, W. Ouyang, T. Kwon, P. Karande, J. Han, Nat. Nanotechnol., **12**, 804-812 (2017).
18. J. Han, H. G. Craighead, *Science*, **288**, 1026-1029 (2000).
19. N. Kaji, Y. Tezuka, Y. Takamura, M. Ueda, T. Nishimoto, H. Nakanishi, Y. Horiike, Y. Baba, *Anal. Chem*., **76**, 15−22 (2004).
20. F. Liang, Y. Guo, S. Hou, Q. Quan, *Sci. Adv.*, **3**, e1602991 (2017).
21. H. N. Chapman, A. K. Ray-Chaudhuri, D. A. Ticher, W. C. Replogle, R. H. Stulen, G. D. Kubiak, P. D. Rockett, L. E. Klebanoff, D. O'Connell, A. H. Leung, K. L. Jefferson, J. B. Wronosky, J. S. Tayer, L. C. Hale, K. Blaedel, E. A. Spiller, G. E. Sommargren, J. A. Folta,F. W. Sweeney, E. M. Gullikson, P. Naulleau, K. A. Goldberg, J. Boker, D. T. Attwood, U. Mickan, R. Hanzen, E. Panning, P. Y. Yan, C. W. Gwyn, S. H. Lee, *J. Vac. Sci. Technol. B, 19* (**6**), 2389-2395 (2001).
22. P. Naulleau, K. A. Goldberg, E. H. Anderson, *J Vac Sci Technol B*, **20**(6), 2829-2833 (2002).
23. Y. Yokota, K. Ueno, S. Juodkazis, V. Mizeikis, N. Murazawa, H. Misawa, H. Kasa, K. Kintaka, J. Nishii, *J. Photochem. Photobiol., A,* **207**, 126-134 (2009).
24. K. Kintaka, J. Nishii, K. Tohge, *Appl. Opt.*, **30**, 489-493 (2000).
25. N. Tohge, R. Ueno, F. Chiba, K, Kintaka, J. Nishii, *J. Sol-Gel Sci.Technol*., **19**, 119-123 (2000).
26. D. J. Kang, J. U. Park, B. S. Bae, J. Nishii, K. Kintaka *Opt. Express*, **11**, 1144-1148 (2003).

Chapter 3.
Label-Free Detection
Using Micro- and Nanofluidic Devices

3.1 Introduction

As mentioned above, various devices exhibiting a number of functions have been developed due to the recent interest in μTAS. Additionally, research focused on complex fields that combine nanotechnology with biotechnology (nanobioanalysis) have attracted increased attention [1]. To effectively detect biomolecules, high sensitivity detection techniques are required along with miniaturization of detection devices. Detection devices generally require a method for labeling a sample with a fluorescent dye or an enzyme to achieve highly sensitive detection [2-11]; however, this approach is labor- and time-intensive and requires expensive reagents. Additionally, physiological activity may be lost as a result of labeling [12, 13]. A label-free detection method that overcomes these problems may prove to be ideal for studying biomolecules. A number of research groups have contributed to the development of label-free detection approaches such as, plasmonic sensing [14-16], nanowire sensing [17], microcantilever sensing [18], whispering gallery mode sensing methods [19], and thermal lens microscopic methods [20, 21]. Although these methods can achieve high sensitivity, they either require immobilization of the molecules that specifically interact with the analyte onto the sensor surface as a pretreatment procedure or they require complicated optical systems.

In this section, a label-free detection technique using nanostructures without any fluorescent molecules or enzymes is discussed. DNA was used as a model biomolecule for this detection.

3.2 Experimental Design

3.2.1 Detection Principle and Measurement System

Our strategy to achieve label-free detection uses diffracted light that is one of the characteristic features of nanochannels. The nanochannels fabricated on a fused silica substrate function as a transmission grating, and the array can obtain the optical diffraction efficiency (signal intensity) corresponding to the refractive index of the sample in the nanochannels (Figure 12). The intensity (diffraction efficiency) of the diffracted light by the diffraction grating can be analyzed by rigorous coupled-wave analysis (RCWA). In this method, the electric field and the magnetic field in the region where light is incident, the region of the diffraction grating, and the region where light is emitted are expanded, respectively, and the conditions under which each tangent component is continuous are imposed. Finally, we solve these parameters to calculate the diffraction efficiency. We demonstrate that the change in the refractive index within the nanochannel alters the diffraction efficiency by expressing the electric and magnetic fields in the grating region.

In the grating region the periodic relative permittivity is expandable in a Fourier series of the form

$$\varepsilon(x) = \sum_{h}^{\infty} \varepsilon_h exp\left(j\frac{2\pi hx}{\Lambda}\right)$$

where Λ is the pitch of the grating structure, j is the imaginary unit, and ε_h is the *h*th Fourier component of the relative permittivity in the grating region, where a complex exists for lossy or non-symmetric dielectric gratings. By assuming the binary grating

$$\varepsilon_h = (n_{wall}^2 - n_{channel}^2)\frac{\sin(\pi hf)}{\pi h}$$

$$\varepsilon_0 = n_{wall}^2 f + n_{channel}^2(1-f)$$

where *f* is the fraction of the grating period occupied by the region of index n_{wall} and ε_0 is the average value of the relative permittivity.

In order to obtain the basis expansions (mode) representing the electromagnetic field of the grating region, the tangential electric (y component) and magnetic (x component) fields may be expressed as the following equations.

$$E_{grating,y} = \sum_i S_{yi}(z) exp(-jk_{xi}x)$$

$$H_{grating,x} = -j\left(\frac{\epsilon_0}{\mu_0}\right)^{1/2} \sum_i U_{xi}(z)\, exp(-jk_{xi}x)$$

Where ϵ_0 is the permittivity of free space, S_{yi}(z) and U_{xi}(z) are the normalized amplitudes of the *i*th space harmonic fields, and k_{xi} represents the x component of the wavenumber vector of *i*th order diffracted light.

From the Maxwell's equation

$$\nabla \times \mathrm{E} = -\frac{\partial B}{\partial t}$$

$$\nabla \times \mathrm{B} = \mathrm{i} + \frac{\partial D}{\partial t}$$

and relational expression

$$\mathrm{B} = \mu_0 H$$

$$\mathrm{D} = \varepsilon\epsilon_0 E$$

in the grating region, it can be expressed as following:

$$\frac{\partial E_{grating,y}}{\partial z} = j\omega\mu_0 H_{grating,x}$$

$$\frac{\partial H_{grating,x}}{\partial x} = j\omega\epsilon_0\varepsilon(x) E_{grating,y} + \frac{\partial H_{grating,z}}{\partial x}$$

The diffraction efficiency is calculated from the Poynting vector representing the directional energy flux of an electromagnetic field. From the above equation, it can be said that the intensity of the

diffracted light depends on the refractive index within the channels.

The system for label-free detection using the periodic nanochannels is illustrated in Figure 13. The incident laser beam (wavelength: 532 nm, OPTO-LINE, Inc., Tokyo, Japan) was passed through an ND filter (VND-50U, Sigmakoki Co. Ltd., Tokyo, Japan) and was modulated by a light chopper (5584A, NF Corporation, Yokohama, Japan) with a modulation frequency at 1013 Hz. The modulated laser beam was focused through an objective lens (×5, Nikon Corporation, Tokyo, Japan) to the nanowall array of the device. The light diffracted by the nanowall array was detected by a photodiode (ET-2030, Electro-Optics Technology, Inc., Traverse City, MI). The diffraction signal was fed into a lock-in amplifier (LI5640, NF Corporation, Yokohama, Japan) to separate and amplify the frequency. The signal was read out by a data logger (TR-V500, Keyence Corporation, Osaka, Japan). As the sample passed through the point of focused laser, the intensity of diffracted light changes, and the detected signal is sent to a data logger.

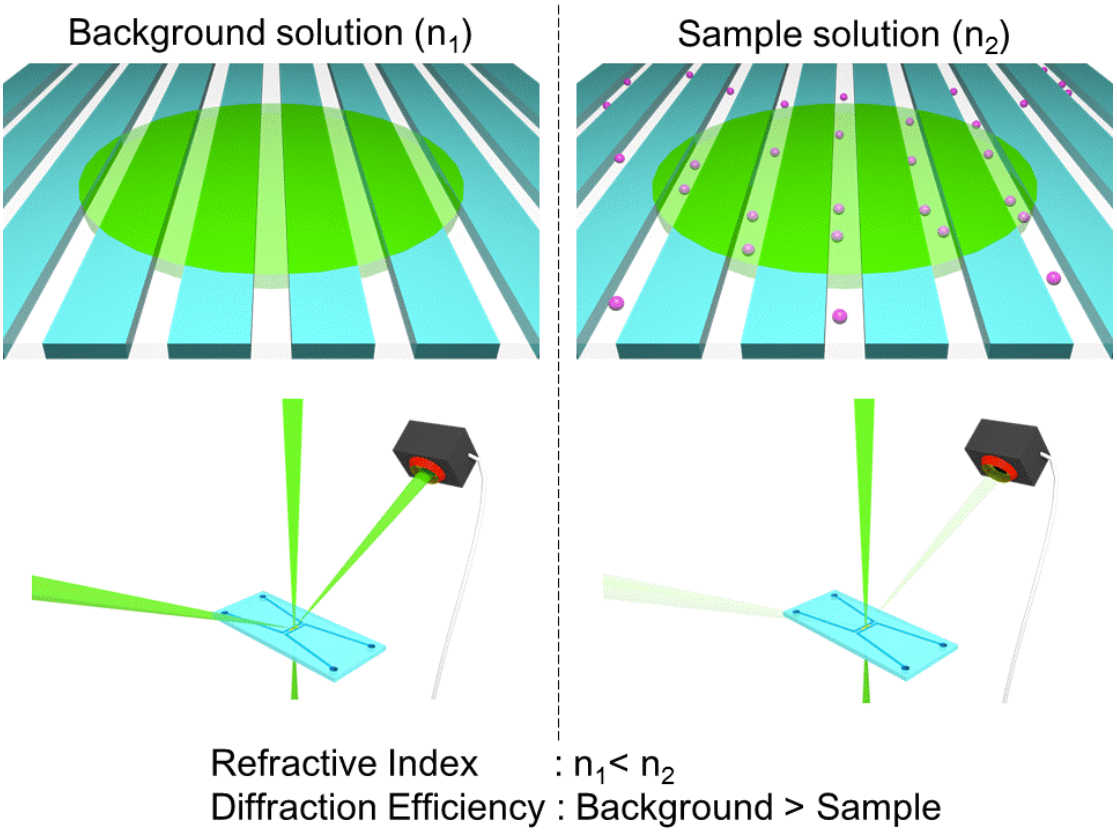

Figure 12. Schematic illustrations of the label-free detection method.

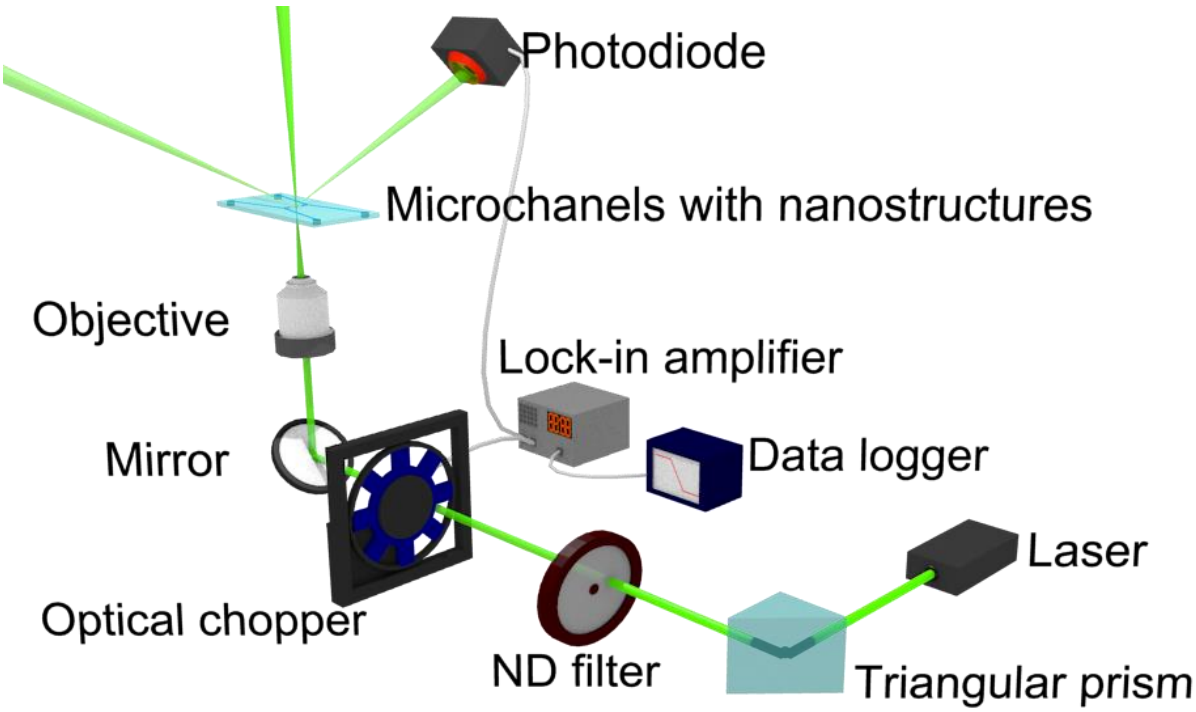

Figure 13. Schematic illustrations of the experimental setup for label-free detection.

3.2.2 Numerical Simulation

We conducted the simulation analysis of the diffraction efficiency of the nanowall array using Diffract MOD (RSoft Design Group Japan KK, Tokyo, Japan) which is based on the rigorous coupled wave analysis (RCWA) method. First, we conducted the simulation for six pure solvents of known refractive index (n=1.3290-1.5241) to confirm the validity of the simulation. Figure 14 shows a cross-sectional view of the device that was used for the simulation analysis. Here we set h as 250 nm, and the wavelength and spot size of the incident light were 532 nm and 4.324 μm, respectively. Second, we set the sample solution refractive index (n=1.33497-1.33501) and the height of the nanowall array as parameters, and we performed the simulation in order to calculate the 1st order diffraction efficiency corresponding to the incident light.

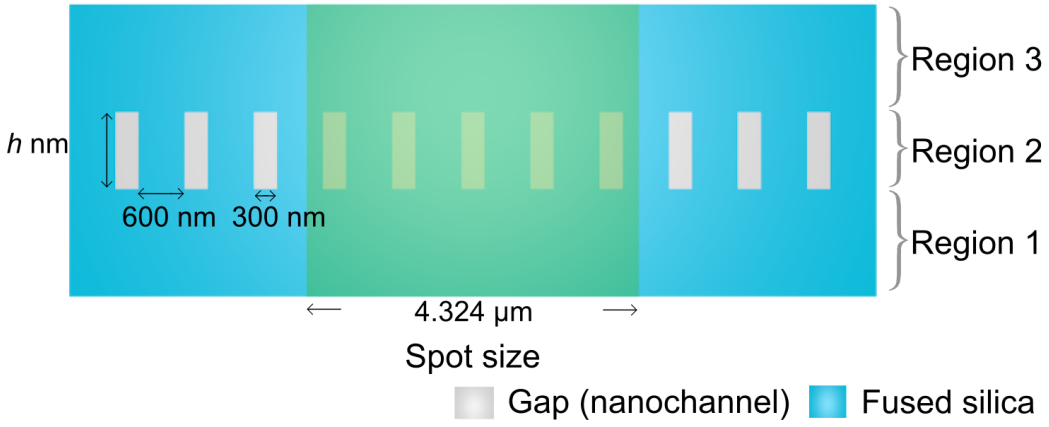

Figure 14. Cross-sectional view of the simulation analysis device. The 532 nm wavelength light and 4.324 μm spot size were both incident from the bottom of this figure. The structures were composed of the incident region (Region 1), diffracted region (Region 2), and emitted region (Region 3). The refractive index outside the structures was set as the refractive index of the air (1.00028).

3.2.3 Label-Free Detection

First, six pure solvents, including methanol (refractive index n = 1.3290), ethanol (n = 1.3614), 2-butanol (n = 1.3978), chloroform (n = 1.4459), *o*-xylene (n = 1.5018), and chlorobenzene (n = 1.5241), with different refractive indexes were introduced into the nanochannels, and the diffracted light intensity was measured. After filling the nanochannels with air, the author introduced each solvent through the inlet hole by dropping the sample solution (2 μL) and filling the channels via the capillary force, and then we measured the transition of the diffraction signal intensity for all devices. Five measurements were made for each solvent.

Second, label-free DNA were measured for two devices. λDNA (Nippon Gene Co., Ltd., Tokyo, Japan) was measured by the nanowall device fabricated by EB lithography. The target sample solution was introduced from the inlet of the device by a syringe pump (World Precision Instruments, Sarasota, FL) (Figure 15). After filling the nanowall array with 1× TE buffer (pH 7.6), the sample solution was introduced, and the author then measured the transition of the diffraction signal intensity. Subsequently, 100 bp DNA was measured by the nanopillar device fabricated by laser interference lithography. The target sample was electrophoretically migrated from the inlet to the detection point. After filling the nanopillar array with 3× TE buffer (pH 8.0), the sample was introduced, and we measured the transition of the signal intensity. Three measurements were made for each sample and both devices.

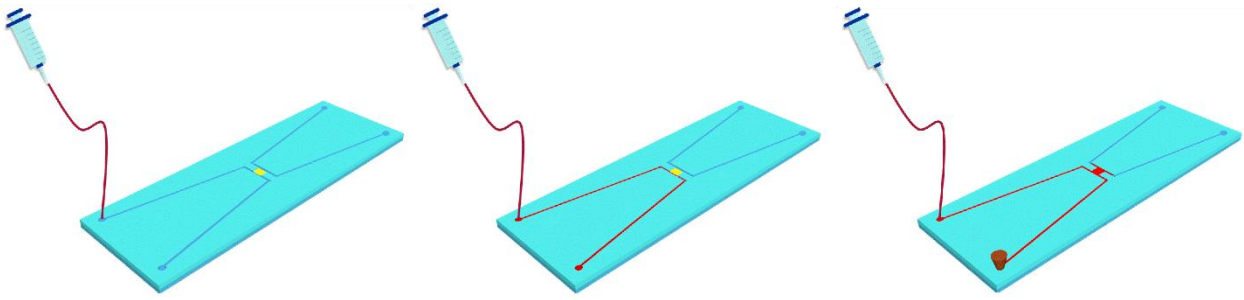

Figure 15. Schematic of sample introduction.

3.2.4 Reagents and Chemicals

Ultrapure water was obtained using a Direct-Q UV system (EMD Millipore Co., Billerica, MA). Ethanol (refractive index n=1.3614), methanol (n=1.3290), 2-butanol (n=1.3978), chloroform (n=1.4459), *o*-xylene (n=1.5018), chlorobenzene (n=1.5241), 2-amino-2-hydroxymethyl-propane-1,3-diol were purchased from Wako Pure Chemical Industries (Osaka, Japan). EDTA was purchased from Dojindo Laboratories., Inc. (Kumamoto, Japan). TE buffer (pH 7.6) was prepared by 10mM Tris-HCl buffer (2-amino-2-hydroxymethyl-propane-1,3-diol, pH7.6 at 25°C) and 1mM EDTA (0.5 M EDTA·2Na, pH7.6 at 25°C). λDNA was purchased from Nippon Gene Co., Ltd. (Toyama, Japan). λDNA soluitons with different concentrations (0.3, 1.5, 3, 6, 9 nM) were prepared by diluting with TE buffer (pH 7.6). Fused silica substrates (n=1.4610 at λ=530.9 nm (from the company's data sheet)) were purchased from Shin-Etsu Chemical Co., Ltd. (Tokyo, Japan).

3.3 Results and Discussion

3.3.1 Diffraction Angle of The Micro- and Nanofluidic Devices

The device prepared in the previous section was used for the experiments in this section. The diffraction angle was examined using a nanowall device. The ability to diffract the laser beam, which the nanochannels intrinsically possess, is governed by the diffraction condition expressed below.

$$pn_1(\sin\theta_0 + \sin\theta_1) = m\lambda$$

Here, *p* is the pitch (900 nm), n_1 is the refractive index of fused silica substrate (1.4610), θ_0 is an angle of incident laser beam (90º), θ_1 is a diffractive angle, *m* is an integer number, and λ is the wavelength of the incident laser (532 nm). The diffracted angle θ_1 values of 23.78º and 54.03º were calculated from the equations for the first order and the second order, respectively. These diffracted light beams are refracted at the interface between the fused silica substrate and the atmosphere, and the refraction angle follows Snell's law

$$n_1 \sin\theta_1 = n_2 \sin\theta_2$$

Considering the refractive index in the atmosphere is 1.00028, we calculated the refraction angle θ_2 values of 36.22º and > 90º for the first order and the second order, respectively. The diffracted light of the first order was visible at 36.22º, and the diffracted light of the second order was total-reflected (Figure 16). We roughly measured the transmissivity for the 532 nm wavelength at each output angle and confirmed that the 532 nm laser beam exhibited some transmittance at ~38º. This indicates that diffracted light was generated as calculated.

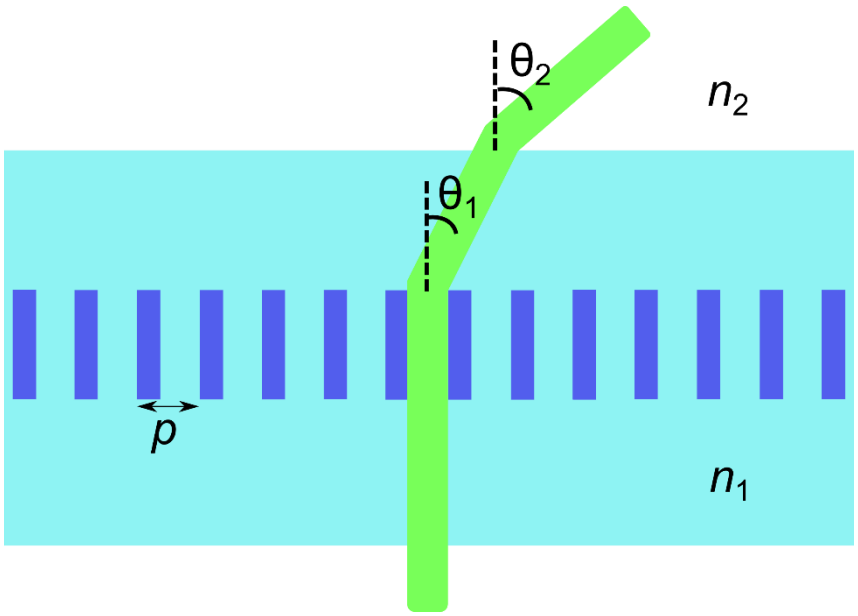

Figure 16. A schematic illustration showing the diffraction of light through the device.

3.3.2 Response to the Refractive Index

We performed label-free detection by introducing various solvents into the nanofluidic diffraction grating (nanowall) to verify the detection ability of our system based on the intensity change of the diffracted light. Here, a nanowall device fabricated by electron beam lithography was used as an initial demonstration. When various solvents were introduced into the device, the refractive index within the nanochannels changed, indicating that the difference in the refractive index between inside of the nanochannels (depending on the sample) and wall of the channels (fused silica substrate [n=1.4610 at λ=530.9 nm, from the manufacturer data sheet]) changed. To achieve proof-of-concept, we monitored intensity changes during the introduction of ethanol molecules as shown in Figure 17, where the refractive index in the nanochannels changed from air to ethanol molecules. Prior to the introduction of ethanol, we detected label-free signals for the air, and then, as we gradually filled the nanochannels embedded in the microchannel with ethanol by capillary force, the intensity of the diffracted light gradually decreased until finally the intensity reached a plateau when the nanochannels were filled. The intensity changes are indicated by S (S was defined as the intensity difference from the initial air-filled state) after sample introduction); $S = \frac{Diffracted\ light\ intensity\ (sample)}{Diffracted\ light\ intensity\ (air)}$), and introducing several solvents in response to the refractive indices of these solvents in Figure 18 indicated that our detection mechanism is primarily based on the change of refractive index. As the refractive indices were close to the refractive index of the device (fused silica), diffraction intensity would decrease. This result was in close agreement with the simulation results, and these results simulated diffraction efficiency changes, E ($E = \frac{Diffraction\ efficiency\ (sample)}{Diffraction\ efficiency\ (air)}$), supporting the validity of this simulation analysis (Figure 19).

Subsequently, the author performed the same experiments and numerical simulations using a device fabricated by a laser interference lithography method to evaluate the performance of the devices (Figure 20 and 21). The results indicated close agreement with the results obtained from

the devices fabricated by EB lithography. This result also indicates that laser interference lithography is useful technique for the fabrication of simple micro- and nanofluidic devices.

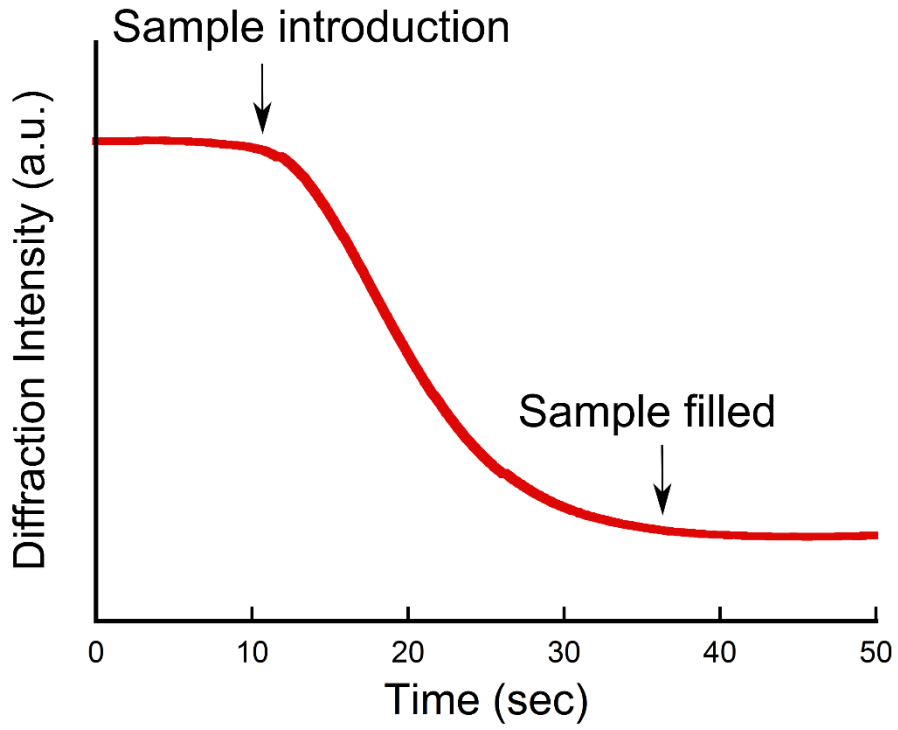

Figure 17. Time-course monitoring of diffraction intensity during ethanol introduction.

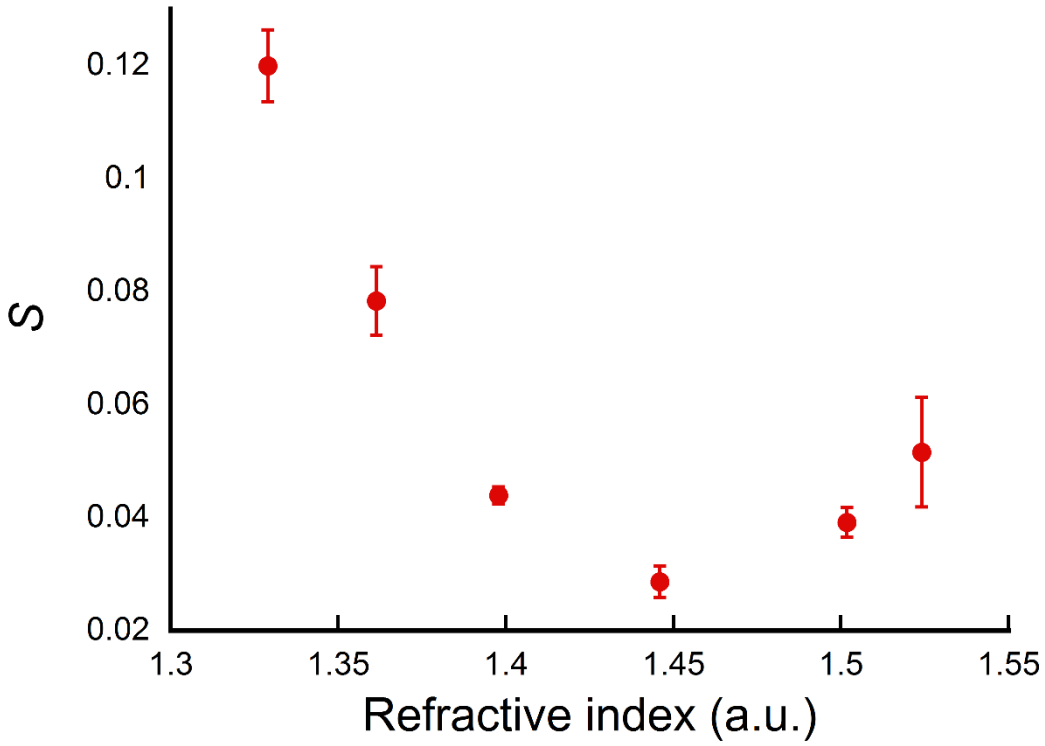

Figure 18. Normalized S plot derived from signal changes during the transit of various liquids. The device fabricated by the electron beam lithography technique was used.

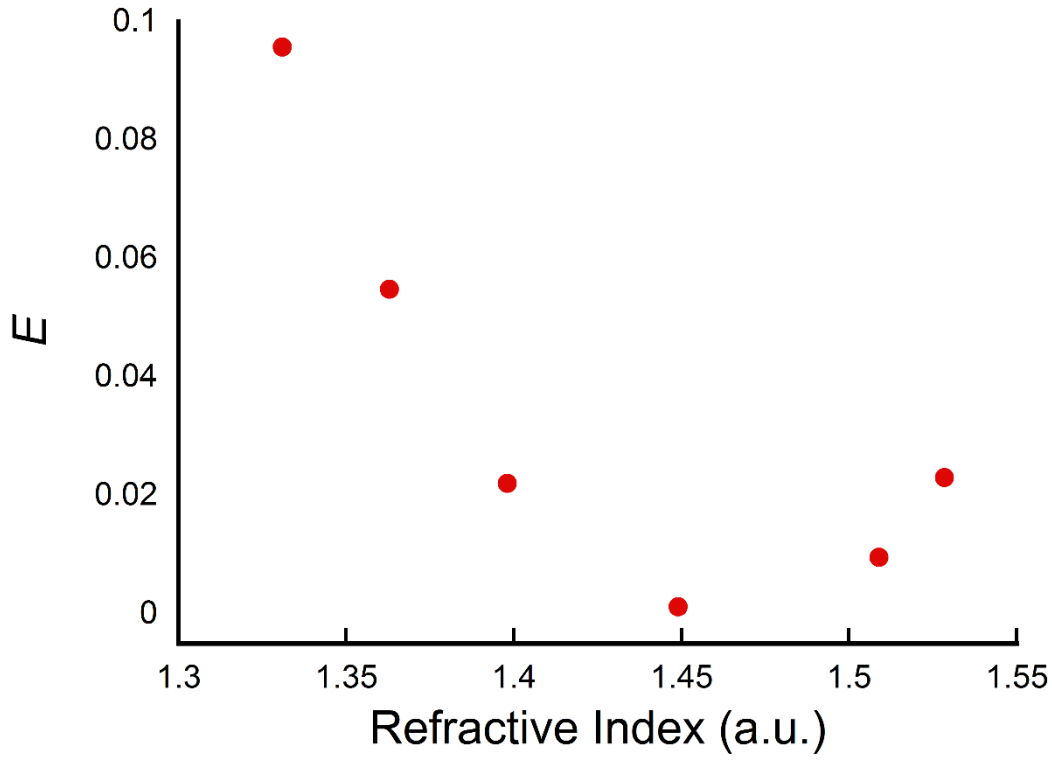

Figure 19. Normalized diffraction efficiency derived from RCWA simulation.

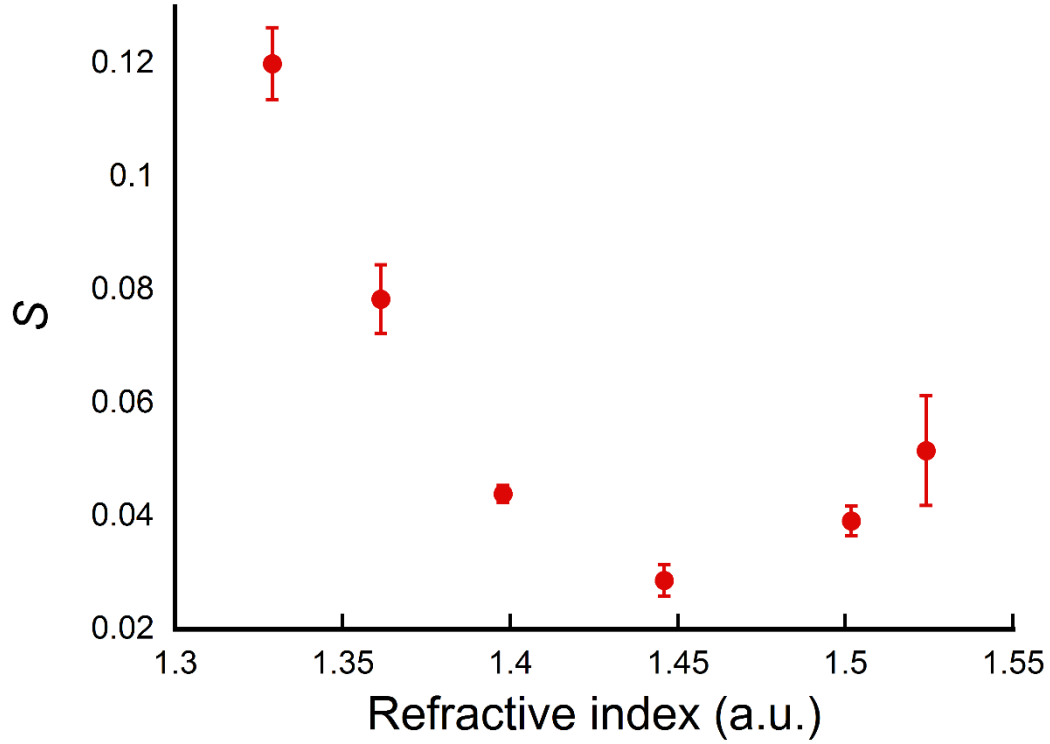

Figure 20. Normalized S plot derived from signal changes during the transit of various liquids. The device fabricated by the laser interference lithography technique was used.

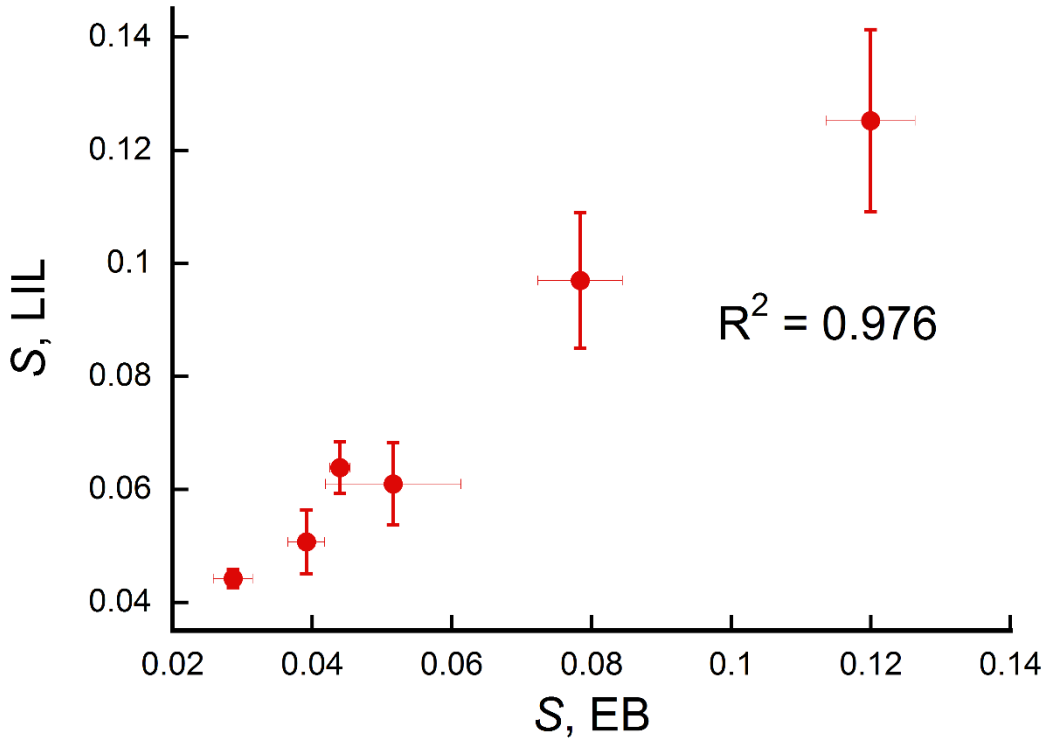

Figure 21. Comparison of the devices fabricated by electron beam lithography (EB) and laser interference lithography (LIL).

3.3.3 Label-Free Detection of Biomolecules

The author performed numerical simulation to consider the effect of the height of the nanowalls. Figure 22 provides the simulation results obtained from the sample solution. The refractive index of the sample solution corresponded to the refractive index of the TE buffer (n=1.33497) and was changed in increments of 0.00001. Here, E was normalized as $E = \frac{Diffraction\ efficiency\ (n=sample)}{Diffraction\ efficiency\ (n=1.33497)}$. The author calculated the diffraction efficiency by setting the parameter h to 150 nm, 200 nm, 250 nm, 500 nm, 1000 nm, and 2700 nm. These results demonstrated that the slope of this line became larger as h became small in either refractive index. Specifically, the lower nanowall exhibited higher sensitivity to changes in refractive index. Table 1 shows the 1st order diffraction efficiency at the TE buffer refractive index corresponding to each h. As shown in Table 1, diffraction efficiency increased when h increased. It was assumed that a higher diffraction efficiency contributed to the improvement of sensitivity. Additionally, when the detection of the diffracted light is considered, it is difficult to detect the light when its intensity is too weak. Interestingly, the limit of detection is in the trade off relationship between these values. In this study, the author fabricated the device with an h of 250 nm when considering these simulation results, the facility for the device fabrication, and the need to achieve efficient sample introduction into the nanowall array.

Based on the simulation results, the author fabricated the nanowall array device with a 600 nm width, 250 nm height, and 300 nm gap. After filling the nanowall array with TE buffer to determine a background value, we introduced each DNA solution, and we measured the changes in diffracted light intensity. Figure 23 shows the relationship between DNA concentration and the variation of the diffracted light intensity. The vertical axis shows the normalized signal intensity $(\Delta S = \frac{Diffracted\ light\ intensity(background) - Diffracted\ light\ intensity(sample)}{Diffracted\ light\ intensity\ (background)})$ and the horizontal axis indicates the DNA concentration. Variation of the diffracted light intensity increased linearly

with increasing DNA concentration. The detection limit of DNA molecules was also evaluated. The detection limit was defined as the number of DNA molecules within the detection volume. From the minimal detected concentration, we calculated the detection limit of DNA molecules to be 0.18 molecules, using a detection volume of about 1 fL. Here, the detection volume was calculated from the spot size of the laser beam and volume of the irradiation region. During the optimization of the nanofluidic design, the detection limit of DNA molecules became lower than that of the higher nanostructures. For the measurement of diffracted light intensity, we used a lock-in amplifier with a time constant of 3 s. The time constant of the lock-in amplifier corresponded to the integration time of the measurement. Specifically, the detection limit of 0.18 molecules indicates that during a 3 s measurement time, there is no DNA molecule in the detection area for 2.46 s and there is a single molecule in the detection area for 0.54 s. This method is an extremely sensitive detection method that can detected a non-fluorescent single molecule such as DNA. The detection of a single non-fluorescent molecule in a solution using a complicated optical setup has been reported, but to the best of our knowledge, there are no reports describing this type of detection using a simple optical setup such as the one described here. For our current study, we used a fused silica substrate. It is possible that sensitivity can be further improved by the use of high-refractive index materials.

Our detection method is based on the refractive index of the sample. Specifically, it can be characterized as a refractometer for a single type of analyte. Our method requires approximately 50 nL to fill the channels with sample. This is a very small sample volume compared to that needed for a conventional highly sensitive refractometer (1 mL). Therefore, our method is advantageous when rare or expensive samples such as biomolecules require detection. Additionally, although the author could recognize the difference between TE buffer and DNA molecules (0.3-9 nM) using the conventional highly sensitive refractometer, the same refractive index was given for all DNA concentrations. Given these results, it is likely that this method

possesses excellent potential to provide a highly sensitive refractometer that requires small sample volumes.

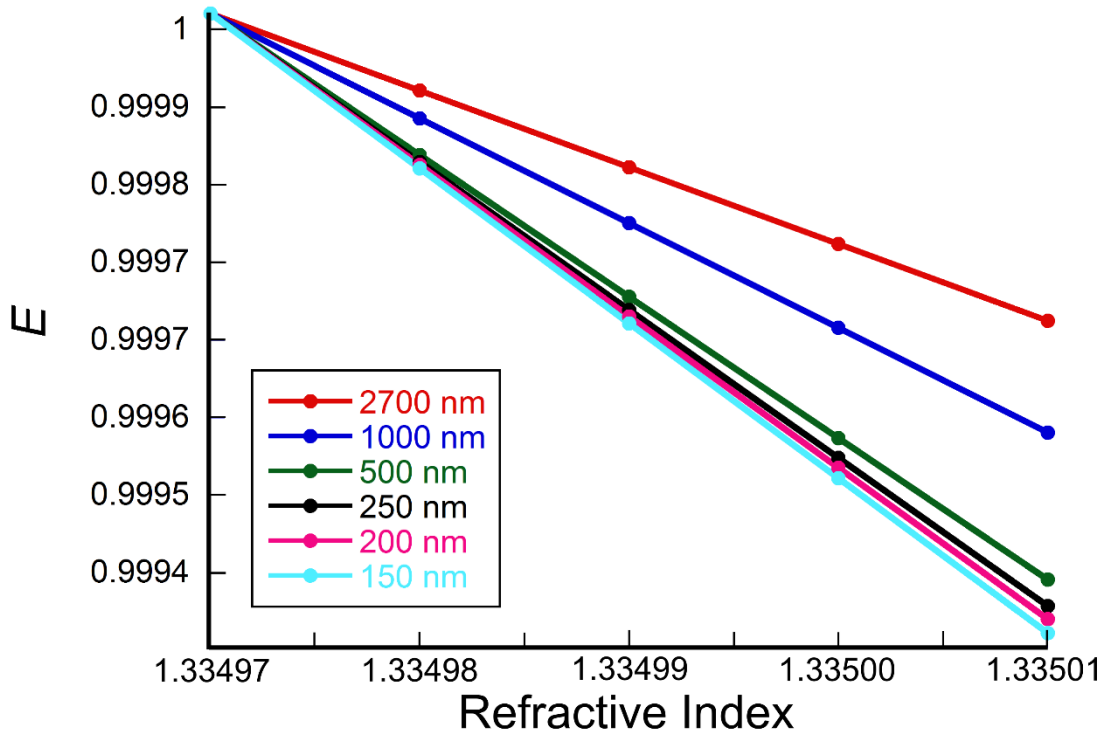

Figure 22. Plots of changes in the diffraction efficiency against the refractive index at various nanowell heights. The vertical axis, *E*, indicates the normalized diffraction efficiency.

Table 1. Simulation results for diffraction efficiency at various nanowall heights. The 1st order diffraction efficiency when TE buffer was introduced to the nanowall array at various nanowall heights.

Height of the nanowalls (nm)	1st order diffraction efficiency (a.u.)
2700	1.43×10^{-3}
1000	1.11×10^{-3}
500	4.02×10^{-4}
250	1.11×10^{-4}
200	6.67×10^{-5}
150	4.17×10^{-5}

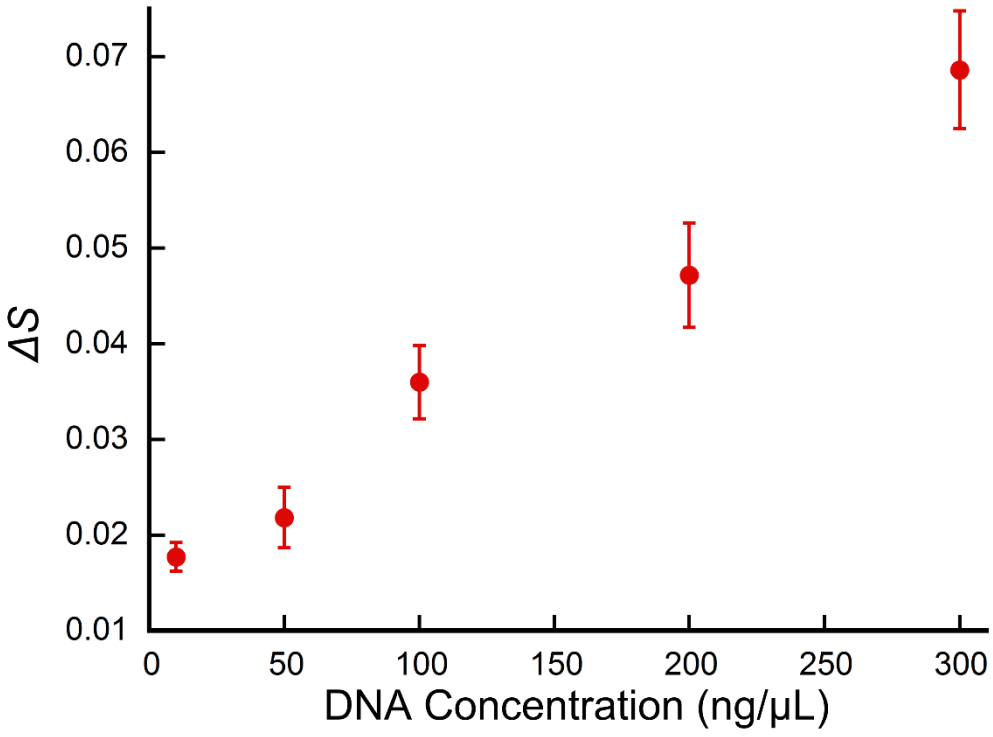

Figure 23. *ΔS* versus concentration of DNA.

3.3.4 Comparison between Nanowall and Nanopillar Devices

The author next investigated diffracted light in the context of nanopillar structures. Laser light was introduced from below the nanopillar device, and transmission diffracted light was projected ono white paper (Figure 24). The incident laser beam was observed to be diffracted in eight directions by the periodically arranged nanopillar structures. The diffracted light of these different diffraction orders can be expressed as (± 1, 0), (0, ± 1), (± 1, ± 1). Among these diffracted lights, diffracted light of (1, 0) was highly sensitive according to the simulation results, and this easily detectable light was used for detection (Figure 25). Figure 26 indicates the simulation and experimental results of the six pure solvents. These results were in close agreement with the results obtained using the nanowall device, and the results were confirmed both by experiments and by simulations (Figure 27). These results supported the validity of the experimental and simulation results obtained from the nanopillar devices. Subsequently, to confirm if biomolecules can be measured with a nanopillar device, a 100 bp DNA strand was used as a model biomolecule. When the DNA reached the detection region, it was observed that the normalized signal intensity increased. Figure 28 shows the calibration curve for DNA. The normalized signal intensity linearly increases with the concentration at this concentration range. These results confirmed that even with the diffracted light from the nanopillar structures, detection is still as sensitive as that observed using the nanowall device.

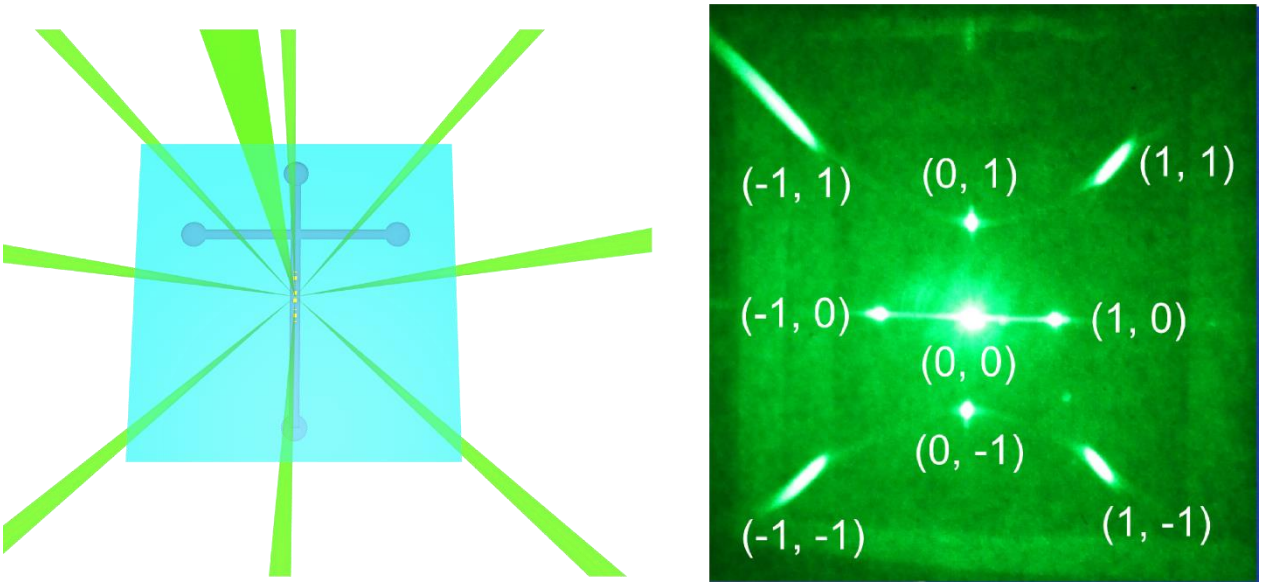

Figure 24. Schematic illustration and an image of the diffracted light from the nanopillar device.

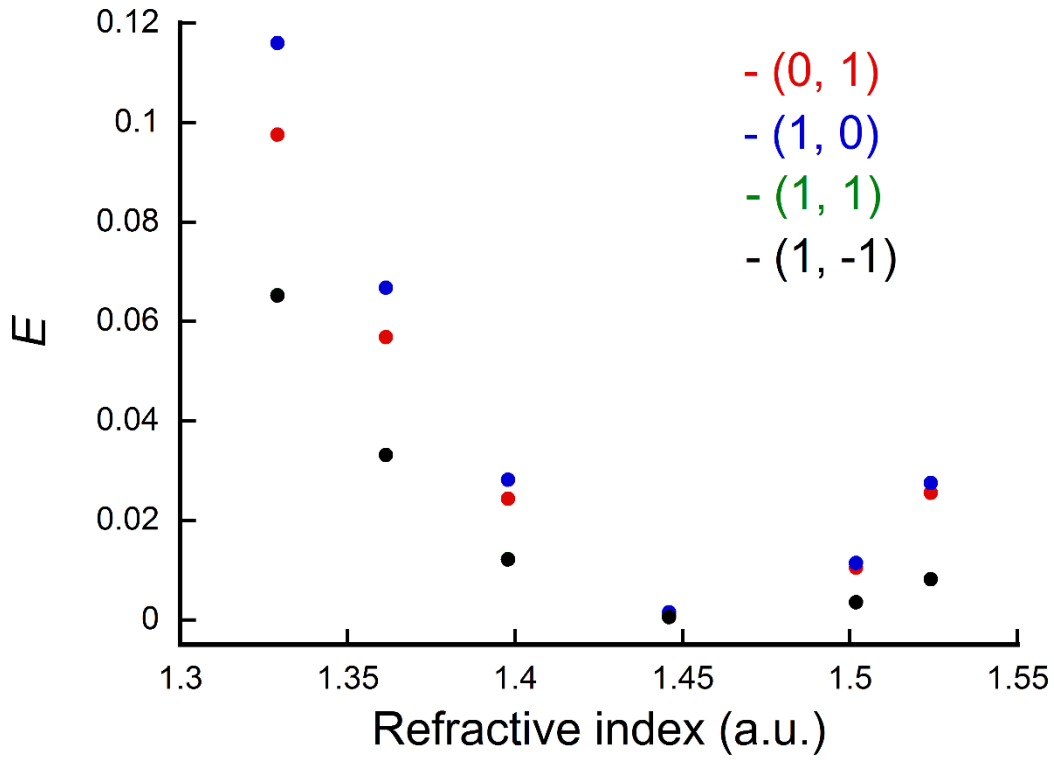

Figure 25. Comparison of refractive index dependence of diffraction efficiency for each diffraction order.

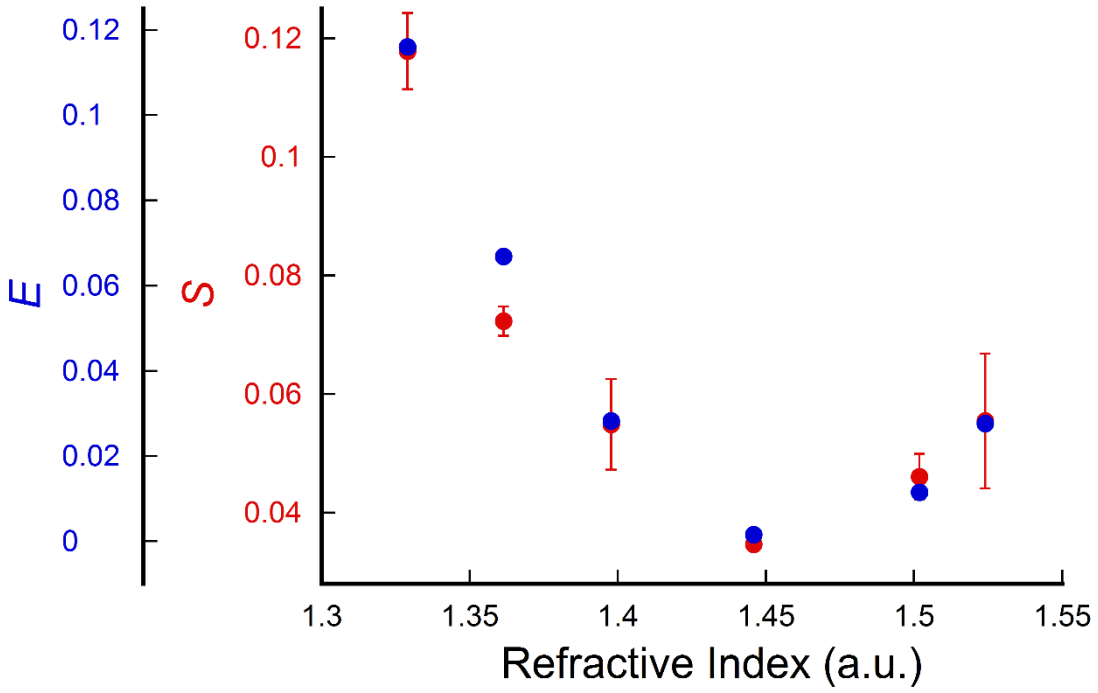

Figure 26. Comparison of normalized intensity (experimental data points; red circles) to diffraction efficiency (simulated data points; blue circles) versus refractive index of the nanopillar device.

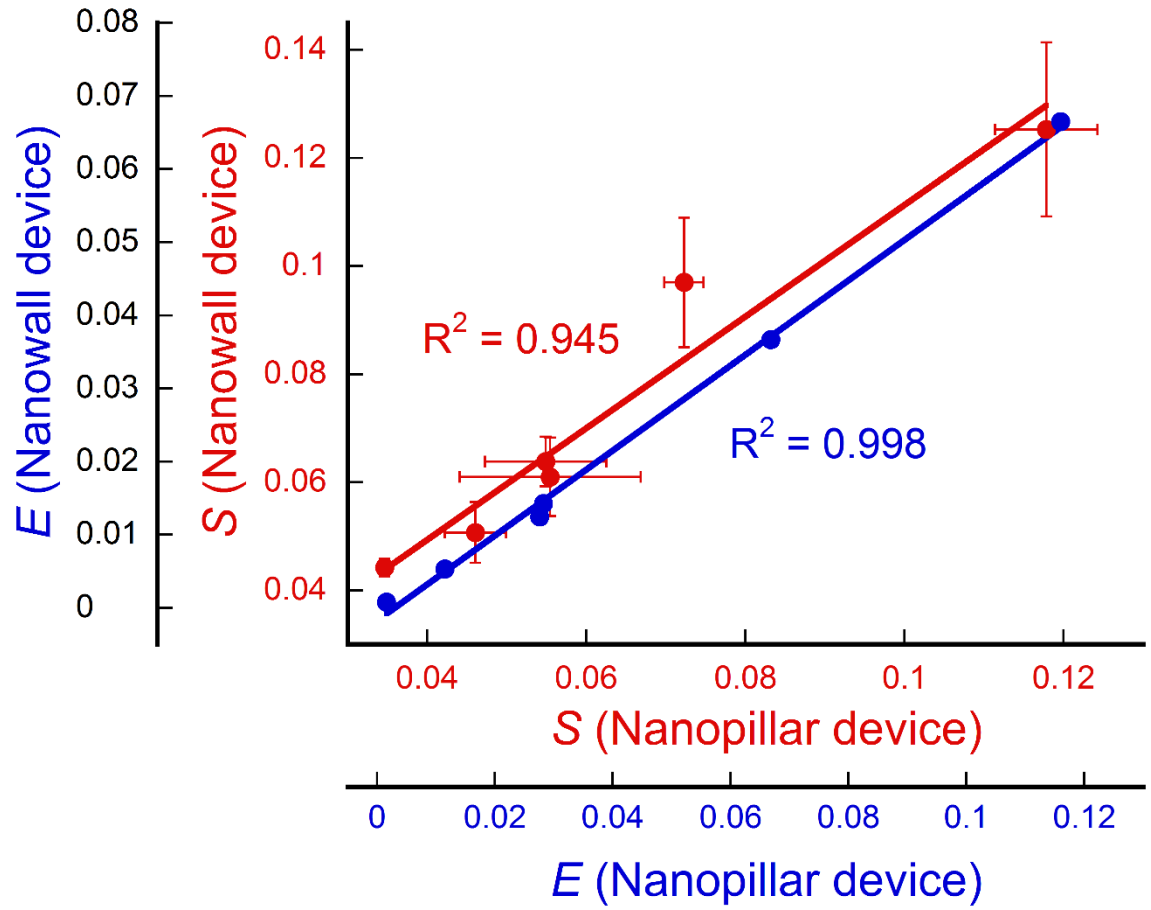

Figure 27. Comparison between the nanowall device and the nanopillar device.

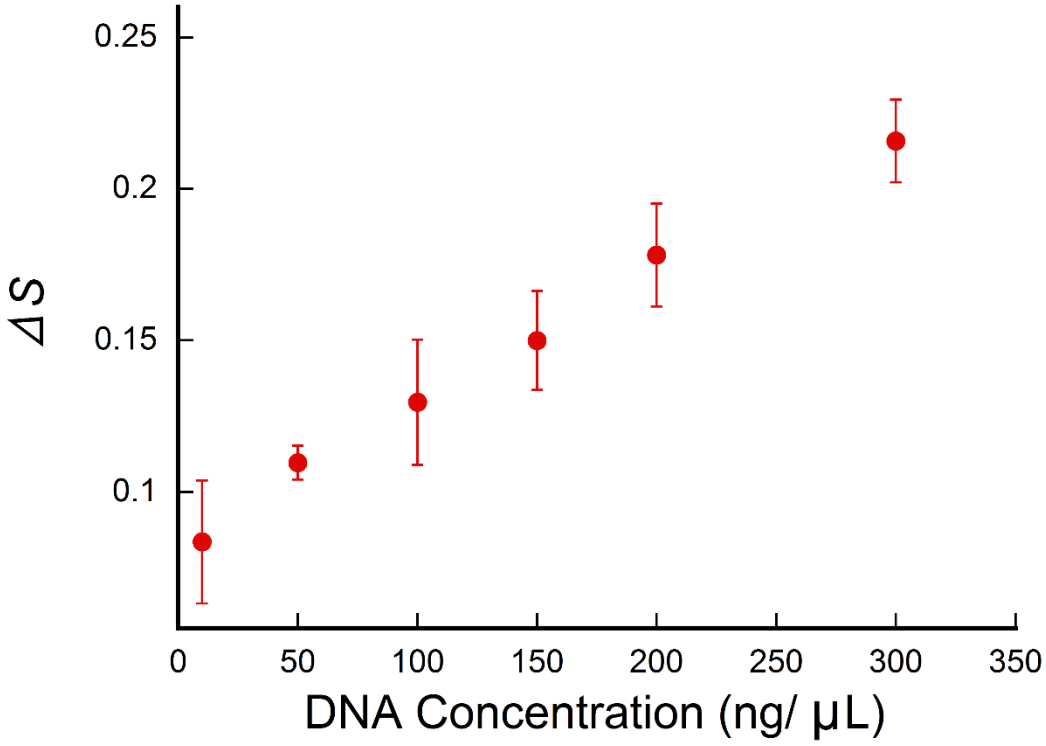

Figure 28. *ΔS* versus concentration of DNA.

3.4 Conclusion

The author have demonstrated a novel label-free detection method using nanofluidic diffraction grating, and this method enables quantitative detection of DNA. The dimensions of a nanowall array we optimized based on simulation analysis, and we could detect label-free DNA at the single molecule level. This method can also detect other label-free biomolecules such as proteins, peptides, and amino acids. Theoretically, this method possesses higher sensitivity due to the large differences in refractive index between the sample and solvent. In this respect, it is believed that DNA is more advantageous than other biomolecules. As mentioned above, the development of a method to monitor the operation of nanofluidic devices that does not require labeling is important. Our method effectively detected biomolecules without labeling, and instead used diffracted light from a nanopillar. The author demonstrated that this detection method possesses potential applicability as a detection method for various nanofluidic devices.

Although this method does not possess sample identification capacity due to its dependence on sample refractive index (a universal detection method), it does possess the capacity to provide sample quantification. By combining separation analysis methods such as electrophoresis or chromatography with our detection methods, it becomes possible to separate and identify biomolecules from small sample volumes. The author anticipates that these integrated devices can be used, not only for fundamental science applications, but also for medical applications.

3.5 References

1. C. V. Mun'delanji, K. Kerman, I. M. Hsing, E. Tamiya, *Nanobiosensors and Nanobioanalyses*. Springer, 2015.
2. M. Ikami, A. Kawakami, M. Kakuta, Y. Okamoto, N. Kaji, M. Tokeshi, Y. Baba, *Lab Chip*, **10**, 3335-3340 (2010).
3. T. H. Kim, J. Park, C. J. Kim, Y. K. Cho, *Anal. Chem.*, **86**, 3841– 3848 (2014).
4. M. L. Chabinyc, D. T. Chiu, J. C. McDonald, A. D. Stroock, J. F. Chrisitian, A. M. Karger, G. M. Whitesides, *Anal. Chem.*, **73**, 4491-4498 (2001).
5. B. H. Weigl, P. Yager, *Science*, **283**, 346-347 (1999).
6. M. L. Adams, M. Enzelberger, S. Quake, A. Scherer, *Sens. Actuators, A*, **104**, 25−31 (2003).
7. J. Han, S. W. Turner, H. G. Craighead, *Phys. Rev. Lett.*, **83**, 1688−1691 (1999).
8. J. Han, H. G. Craighead, *Science*, **288**, 1026-1029 (2000).
9. N. Kaji, Y. Tezuka, Y. Takamura, M. Ueda, T. Nishimoto, H. Nakanishi, Y. Horiike, Y. Baba, *Anal. Chem.*, **76**, 15−22 (2004).
10. Y. Xu, Q. Wu, Y. Shimatani, K. Yamaguchi, *Lab. Chip*., **15**, 3856-3861 (2015).
11. S. H. Ko, D. Chandra, W. Ouyang, T. Kwon, P. Karande, J. Han, Nat. Nanotechnol., **12**, 804-812 (2017).
12. F. Liang, Y. Guo, S. Hou, Q. Quan, *Sci. Adv.*, **3**, e1602991 (2017).
13. J. Romanowska, D. B. Kokh, R. C. Wade, *Nano Lett.*, **15**, 7508-7513 (2015).
14. M. A. Cooper, *Nat Rev Drug Discov*, **1**, 515-528 (2002).
15. S. Hana, Z. Shile, M. D. Aimee, G. David, W. Kai, H. Jiri., *Anal. Chem.*, **82,** 10110–10115 (2010).
16. M. Piliarik, M. Vala, I. Tichy, J. Homola., *Biosens. Bioelectron.,* **24**, 3430-3435 (2009).
17. C. M. Lieber, J. Hahm, *Nano Lett,* **4**, 51-54 (2004).
18. G. Shekhawat, S. H. Tark,V. P. Dravid, *Science,* **311**, 1592-1595 (2006).

19. F. Vollmer, S. Arnold, *Nat. Methods*, **5**, 591-596 (2008).

20. M. Tokeshi, M. Uchida, A. Hibara, T. Sawada, T. Kitamori, *Anal. Chem.*, **73**, 2112−2116 (2001).

21. F. Kitagawa, Y. Akimoto, K. Otsuka, *J. Chromatogr., A*, **1216**, 2943– 2946 (2009).

22. M. G. Moharam, E. B. Grann, D. A. Pommet, *J. Opt. Soc. Am.*, **12**, 1068– 1076 (1995).

Chapter 4.
Separation Analysis
Using a Nanopillar Device

4.1 Introduction

Separation analyses of biomolecules (DNA, proteins, and amino acids) are important in various fields such as fundamental biology and medical diagnosis [1-16]. Although gel-based separation has been actively used for some time, their separation ability is limited, and they require a large sample volume and more time. In the 1990s, capillary electrophoresis and microchip electrophoresis techniques, which are faster and can be miniaturized and parallelized, were developed and greatly improved parameters such as sample volume, separation speed, and throughput [4, 5, 11, 13, 16]. Additionally, these methods can be easily combined with other analytical methods such as mass spectrometry [16]. In recent years, separation technology using nanostructures has been reported, and it has been observed that a unique separation mechanism specific to the nanospace exists [17-33]. J. Han *et al*. reported the "entropic trap" in 1999, N. Laachi *et al*. theoretically predicted it in 2007 and T. Yasui *et al*. experimentally demonstrated "torque assisted escape". Larger DNA strands migrate faster than short DNA strands for both phenomenon, but the underlying mechanisms are different. In the former the channel space is 100 nm or less, which is smaller than the gyration radius of DNA, and the longer DNA strand has a larger contact area with the channel. The chance to escape from the entropy trap is therefore large. In the latter, where the channel possesses a large number of cylinder structures aligned parallel to the channel, longer DNA strands migrate predominantly by electric-field-induced torque and smaller DNA strands are greatly affected by rotational diffusion. Thus, the longer DNA strands migrate faster than the smaller DNA strands in both conditions. In the restricted nano-space, the environments exert a large effect on separation. In general, a highly sensitive fluorescence method was used for monitoring the separation within the nanofluidic channel as previously mentioned. This is strongly affected, however, by labeling agents present in separation using the above mentioned nanostructures. To investigate the separation mechanism, it is necessary to develop a monitoring method that does not require any labeling the sample.

In this section, label-free monitoring of DNA separation using nanostructures is reported. Cylinder shaped structures (nanopillar) were used as the separation mechanism was known in detail. Figure 29 shows the conceptual illustration of this research.

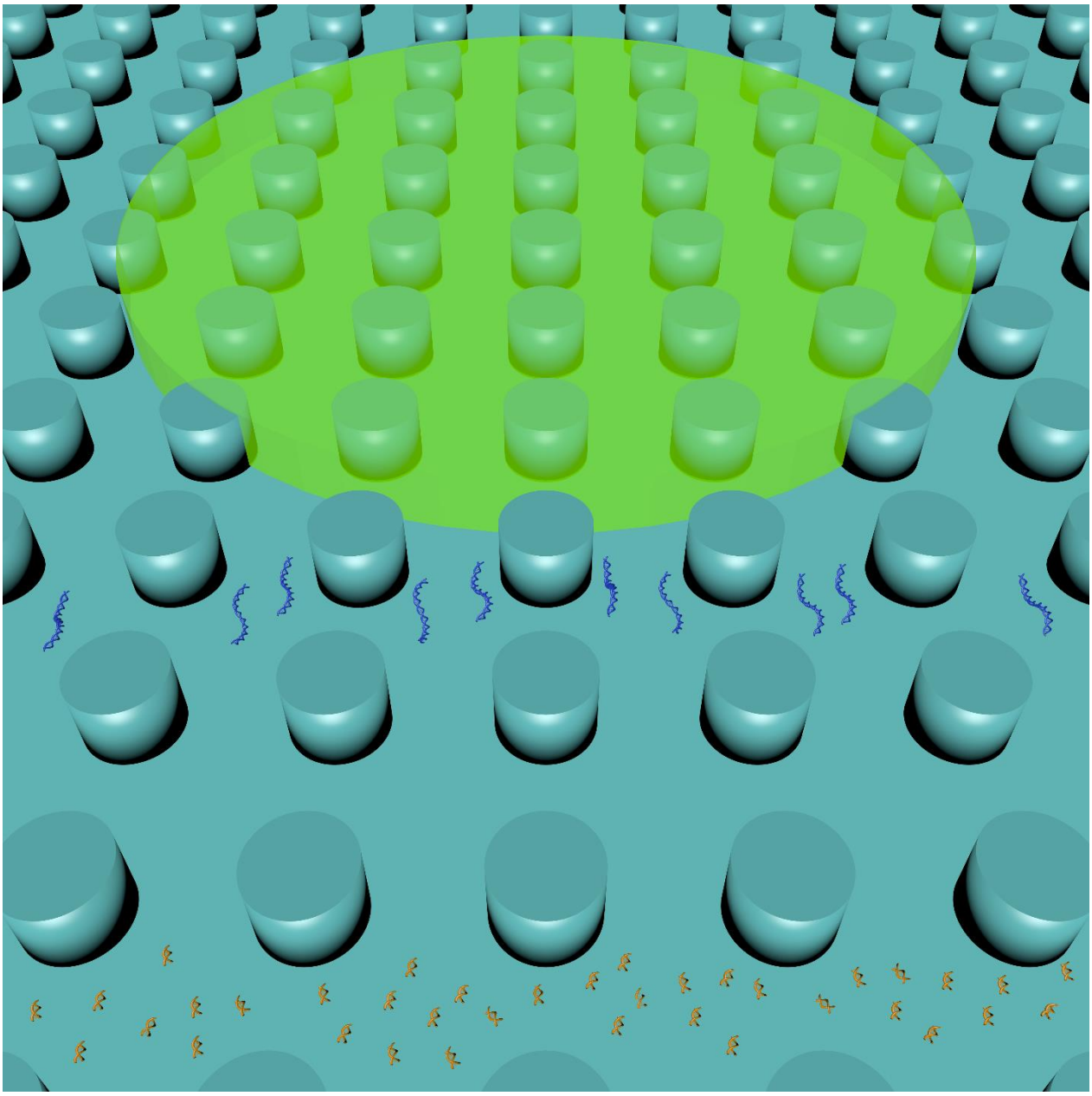

Figure 29. Conceptual illustration of this chapter. DNA strands were separated by size using nanopillar structures and detected using diffracted light from the nanopillar structures.

4.2 Experimental Design

4.2.1 Electrophoresis

Variously sized DNA strands (100 bp and 1 kbp) were used for DNA separation. DNA was prepared at a concentration of 200 ng/μL, and separation was monitored at 5 mm downstream from the cross section of the channels. For the fluorescence observation experiments, each DNA solution was stained with several concentrations of intercalator (YOYO-1, Thermo Fisher Scientific). The dye-to-base ratio of the final working solution was ~1:30, 1:60, 1:100, and 1:150. The fluorescence observation apparatus was constructed by replacing the laser of the label-free detection system. A laser (488 nm) was expanded with a beam expander, introduced into a microscope, and the fluorescence of individual DNA molecules was captured by an EM-CCD camera. Recorded videos on a DV tape (DSR-11, SONY, Tokyo, Japan) were analyzed later by an image-processing software (Cosmos32, Library Inc., Tokyo, Japan).

4.2.2 Chemicals and Reagents

Ultrapure water was obtained using a Direct-Q UV system (EMD Millipore Co., Billerica, MA). EDTA was purchased from Dojindo Laboratories., Inc. (Kumamoto, Japan). TE buffer (pH 7.6) was prepared by 10mM Tris-HCl buffer (2-amino-2-hydroxymethyl-propane-1,3-diol, pH7.6 at 25°C) and 1mM EDTA (0.5 M EDTA·2Na, pH7.6 at 25°C). 5×TBE buffer was prepared from 0.445 M Tris-HCl buffer, 10 mM EDTA, 0.445 M boric acid and diluted with water to 3×TBE buffer.

4.3 Results and Discussion

4.3.1 Size-Based DNA Separation Using a Nanopillar Device

In this study, size-based separation of DNA using a nanopillar device was performed. It had been reported that the nanopillar arrays within the microchannel, which have nanometer-scale pillar structures, were used as matrices for DNA and protein separation instead of natural or synthetic polymers. It was also reported that the geometric pattern of the nanopillar array can influence the separation mode. When the nanopillars were aligned in a tilted orientation to the microchnnels, the molecular sieve effect occurred and the shorter DNA migrated more rapidly than the longer DNA. Conversely, when the nanopillars were aligned parallel to the microchannels, this provided nonequilibrium transport of DNA molecules, and the longer DNA migrated more rapidly than the shorter DNA. In this study, size-based DNA separation using paralleled aligned nanopillars in a square array pattern was demonstrated.

For the separation at the square nanopillar, the effect of DNA molecule transport can be quantitatively expressed by considering the rotational Péclet number that represents the relative effect of dielectric rotation and rotational diffusion. The rotational Péclet number can be obtained as follows.

The time for the molecular diffusion over the time for convection under AC electric fields across a single unit distance of the repeated structures, d_u, which corresponds to the pitch of a nanopillar array, can be represented by the Péclet number.

$$\mathrm{Pe} \equiv \frac{d_s/D}{d_u/\mu_o E_s}$$

Here, d_s is the distance of the nanopillar spacing, D is the molecular diffusion constant, μ_o is the electrophoretic mobility of DNA molecules in free solution and E_s is the electric field across the nanopillar. An increase in molecular diffusion by applying high electric fields decreases the

separation resolution; however, concerning semi-rigid DNA molecules, they are expected to migrate in a manner that is affected by electrorotation between consecutive nanopillars under strong electric fields. To extend the above equation to finite-sized DNA molecules, Laachi *et al*. included the factor of rotational diffusion, D_r, into the equation. (24) This led to a critical lower bound of the electric field when considering the probability of an acceptable conformation to exit and enter the space between the nanopillar. As rotational diffusion prevents DNA molecules from reaching the next nanopillar spacing, the DNA molecules do not simply migrate straight between the nanopillar spaces. To escape from this conformation, these DNA molecules must overcome the rotational diffusion through continued rotational diffusion and electric-field-induced torque (electrorotation) (Figure 30). To quantify the effect of these rotations, the rotational Péclet number, Pe_r, is derived as the following equation.

$$Pe_r = \frac{M}{k_B T}$$

$$\begin{aligned} \mathrm{M} &= (F_n - F_s)L \\ &= \hat{q}(E_n - E_s)L^2 \end{aligned}$$

Here, $k_B T$ is the Boltzmann factor, M is the electric-field-induced torque estimated from the electric field gradient acting on a DNA molecule near an entry or an exit of the nanopillar spacing, F_n and F_s are the exerted force on the two ends of the DNA molecule, L is the contour length of the DNA, $\hat{q}$ is DNA charge per unit length, and E_n and E_s are the electric fields interposed by the nanopillars. Spacing ratio, δ can expressed as follows.

$$\begin{aligned} \delta &= \frac{d_u - d_s}{d_s} \\ &= {E_n}/{E_s}. \end{aligned}$$

Considering the resistances in series, the rotational Péclet number can be described as follows.

$$Pe_r = \left(\frac{1-\delta}{1+\delta}\right)\left(\frac{\hat{q}E_{av}L^2}{k_B T}\right) \qquad (1)$$

E_{av} is the averaged electric field. Figure 31 shows calculated results of Pe_r with respect to the

electric field of the DNA (100 bp and 1 kbp) used in the experiment. T. Yasui *et al*. reported that DNA is efficiently separated under the condition that the Pe_r of shorter DNA is below 0.1 and larger DNA is above 0.1. Additionally, the resolution of separation is proportional to the applied electric field. In this study, the voltage was set to E = 200 V/cm for the separation, and this satisfies the above conditions. Figure 32 shows the obtained electropherogram. As expected, we could separate the mixture of 100 bp and 1 kbp DNA at 200 V/cm. These result indicated that it is possible to separate the DNA even with the nanopillar device fabricated by laser interference lithography techniques. Additionally, the YOYO-1 that is used for labeling the DNA is concentration-dependent. As the concentration of YOYO-1 decreases, migration speed increases. This is likely due to changes in the effective charge of the DNA-YOYO-1 complex that is dependent upon the amount of YOYO-1 that intercalates into DNA. Similar phenomena have been reported for gel electrophoresis and capillary electrophoresis, (34-38) and it was possible to confirm these hypotheses using nanopillar devices.

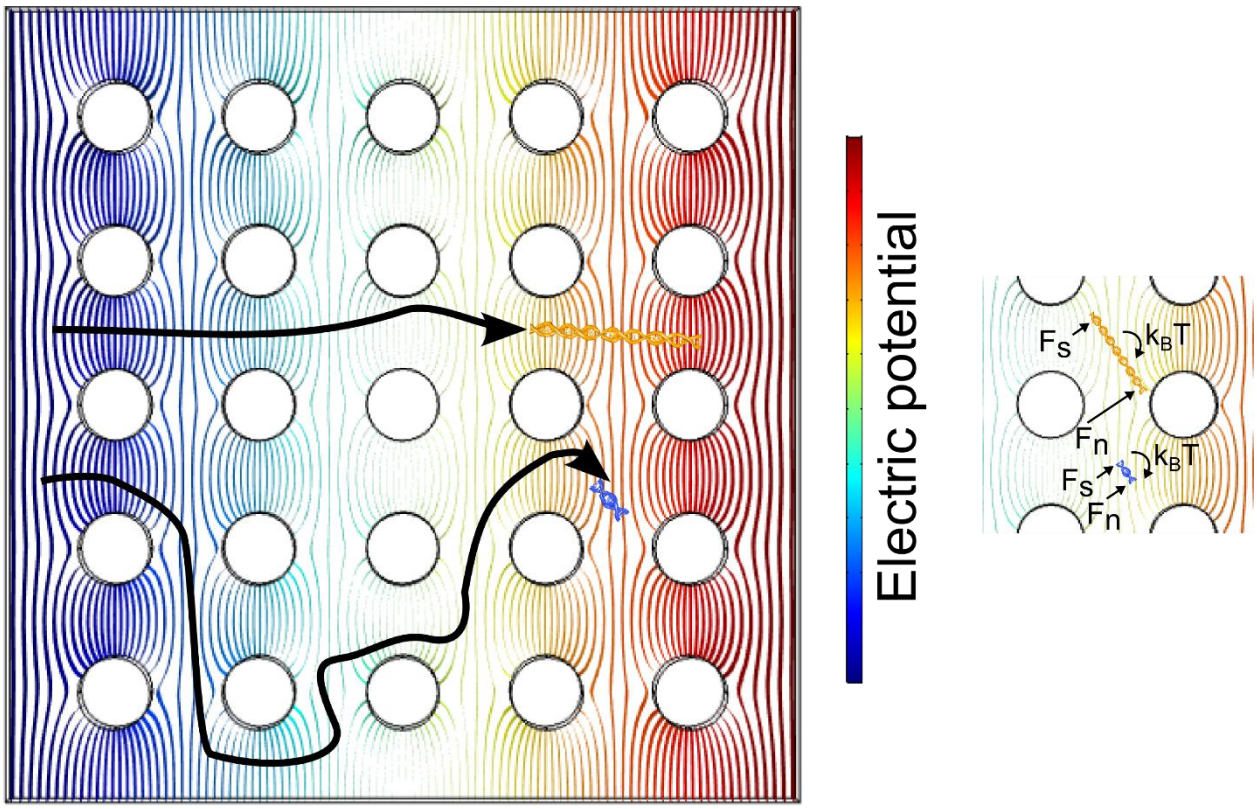

Figure 30. Schematic of the simulated field potential of the nanopillars arranged in the square array pattern. In this nonuniform electric field, the predicted trajectory and the rotational force of DNA molecules are depicted by black arrows.

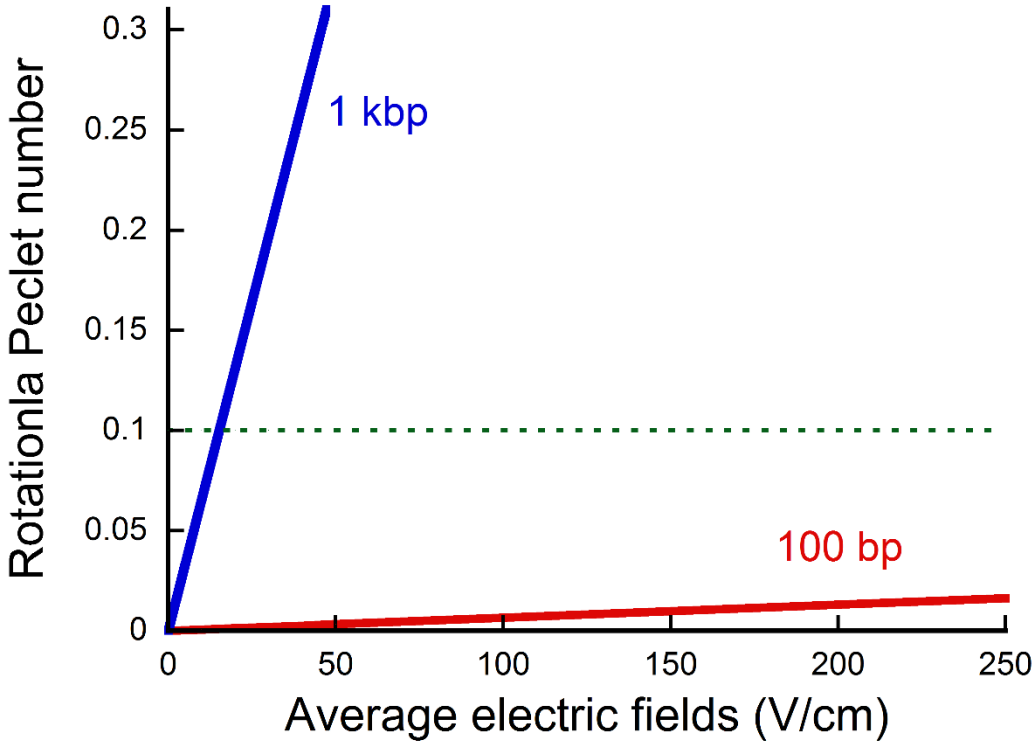

Figure 31. Relationship between the rotational Péclet number and the electric field for 1 kbp and 100 bp DNA molecules. The dotted line indicates $Pe_r = 0.1$.

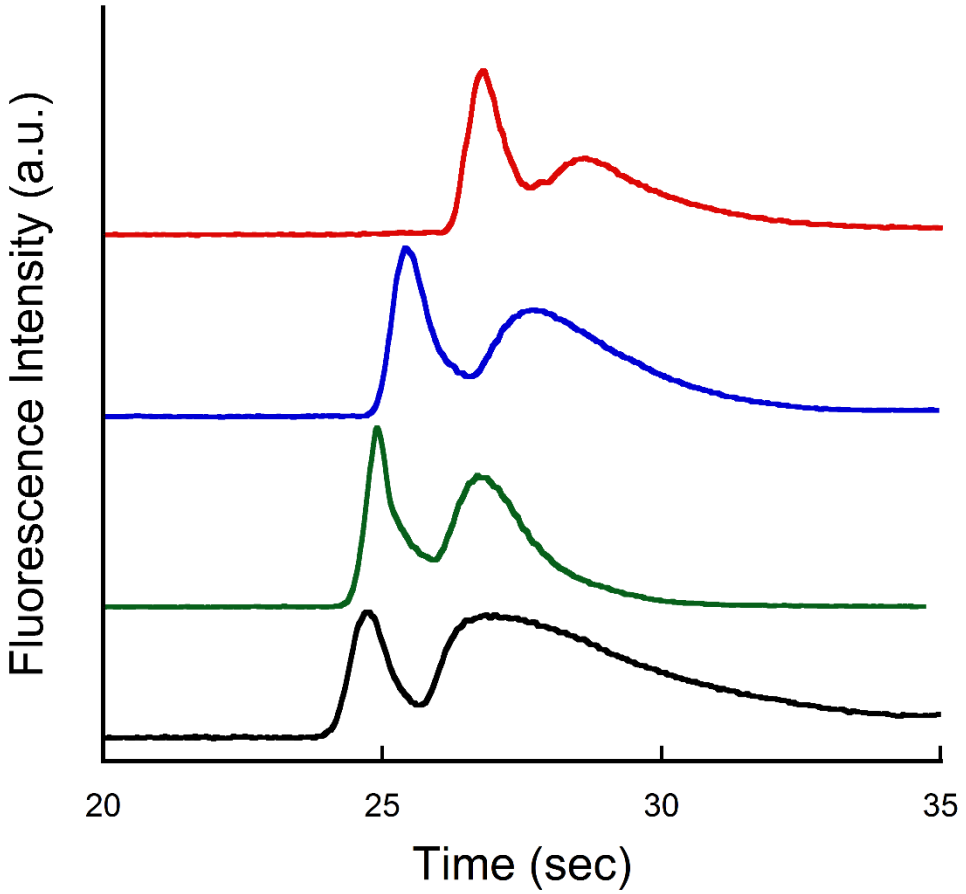

Figure 32. Electropherogram of the mixture of 100 and 1 kbp DNA at various YOYO-1 concentrations (Dye-to-base ratio, 1:30 (red), 1:60 (blue), 1:100 (green), 1:150 (black)).

4.3.2 Separation and Label-Free Detection

Label-free monitoring of size-based DNA separation using the fabricated nanopillar device was demonstrated. This diffraction-based measurement system utilizes a lock-in amplifier for signal measurement. The time constant of the lock-in amplifier corresponds to the integration time of signal sampling. Therefore, a longer time constant enables the acquisition of a higher signal-to-noise signal. For these measurements, however, it is desirable to acquire plenty large amount of signal when the bands separated by electrophoresis pass through the fixed detection point. For these measurements, the time constant of the lock-in amplifier was set to 3 ms to account for S/N and migration speed. Figure 33 illustrates an electropherogram of a DNA mixture observed by label-free detection. Two peaks were observed, and both peaks were fitted based on Gaussian fitting. The later peak is broader, and it exhibits diffusion-based migration, as expected. Figure 34 presents electropherograms of samples containing 100 bp, 1 kbp, or no DNA (TE buffer only), respectively. The signal was smoothed using the 5% weight moving average method. Although the resolution was lower compared to that of the fluorescence detection method, the two peaks derived from 100 bp and 1 kbp were still detectable. Subsequently, comparison using fluorescence observation was performed. A comparison was made between the results of the dye-to-base 1:150 with the lowest amount of fluorescence dye with the highest migration speed among the fluorescence observations and the result of label-free detection (Figure 35). It was observed that DNA migrated more rapidly than DNA labeled with YOYO-1. This is due to the fact that the effective charge of the unlabeled DNA is larger than the labeled DNA as described above, and these differences were successfully detected using this detection method. Additionally, in the case of nanopillar separation, torque assisted escape must be taken into account and this is believed to contribute to the overall effects. It is considered that the charge $\hat{q}$ and the contour length L of the DNA were affected by the rotational Péclet number from equation (1). The effective charge was reduced by complex formation of YOYO-1, a cationic intercalator, with DNA molecules.

Complex formation is expected to increase size, however, it have been reported that there is less of an effect at such a low concentration of YOYO-1. (34) From the above observations, it is believed that Pe_r decreases as the concentration of YOYO-1 increases. Since this reduction represents a decrease in the torque assisted effect, longer DNA may be more affected by high concentrations YOYO-1. This phenomenon was experimentally confirmed by comparing the average time for each DNA peak to reach the detection point (Figure 36, 37 and 38). This could not be demonstrated experimentally due to the differences in detection sensitivity for each measurement; however, our results suggest that separation analysis with high resolution can be performed without labeling.

Comparing the electropherogram obtained by our label-free detection system with the fluorescence observation results, the peak of the label-free signal is broad. We speculated that this is likely due to two reasons. One is that the sensitivity of the current label-free detection system is lower than current fluorescence techniques. For these measurements, the difference between the obtained signal and the background signal was very small. Therefore, the obtained electropherogram was broad. Second, it is believed that the change in the refractive index is small as compared to the change in the fluorescence amount. Improvement of sensitivity can be achieved by optimization of nanostructure and improvement of the optical system (high intensity light source, introduction of heterodyne detection system, etc.). It is likely that it is possible to achieve detection sensitivity comparable to fluorescence detection, even if the refractive index change is subtle.

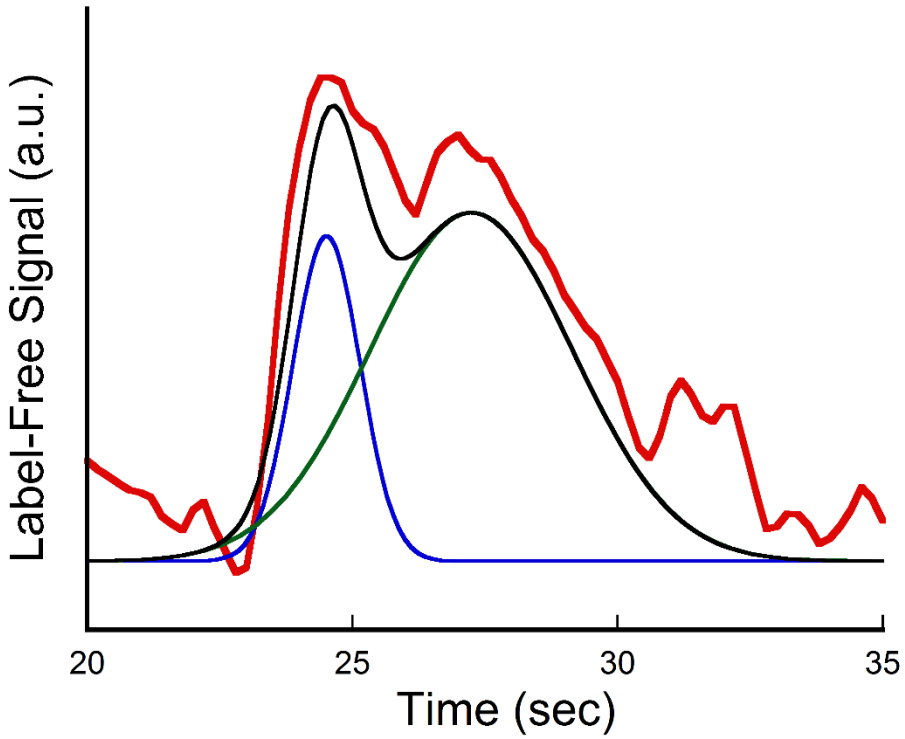

Figure 33. Electropherogram of label-free DNA (red) and results of peak fitting (First peak, blue; Second peak, green; Synthetic peak, black).

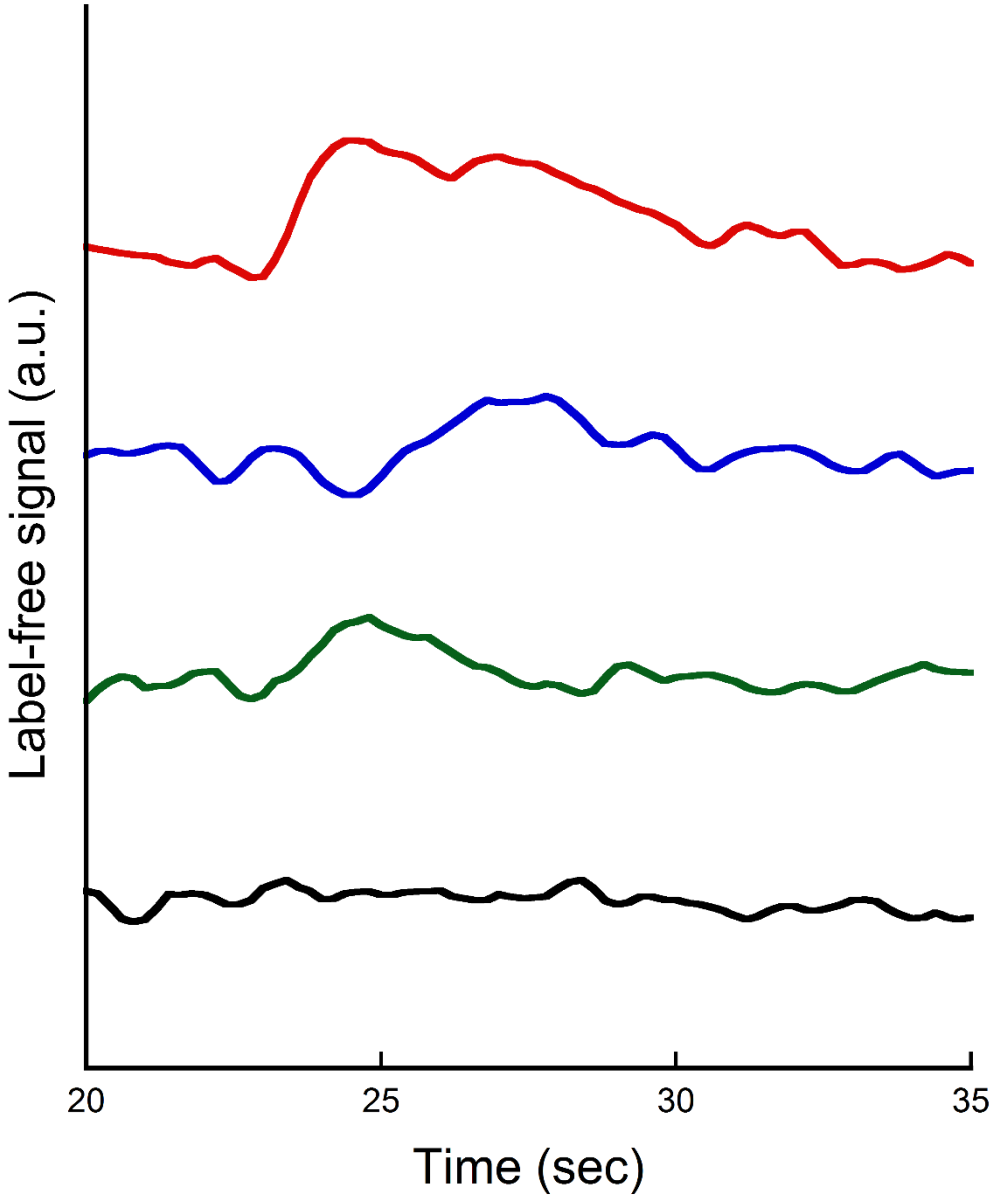

Figure 34. Electropherogram of label-free DNA. Electropherogram of a mixture of 100 bp and 1 kbp DNA (red), 100 bp only (blue), 1 kbp only (green), and no DNA (TE buffer) (black).

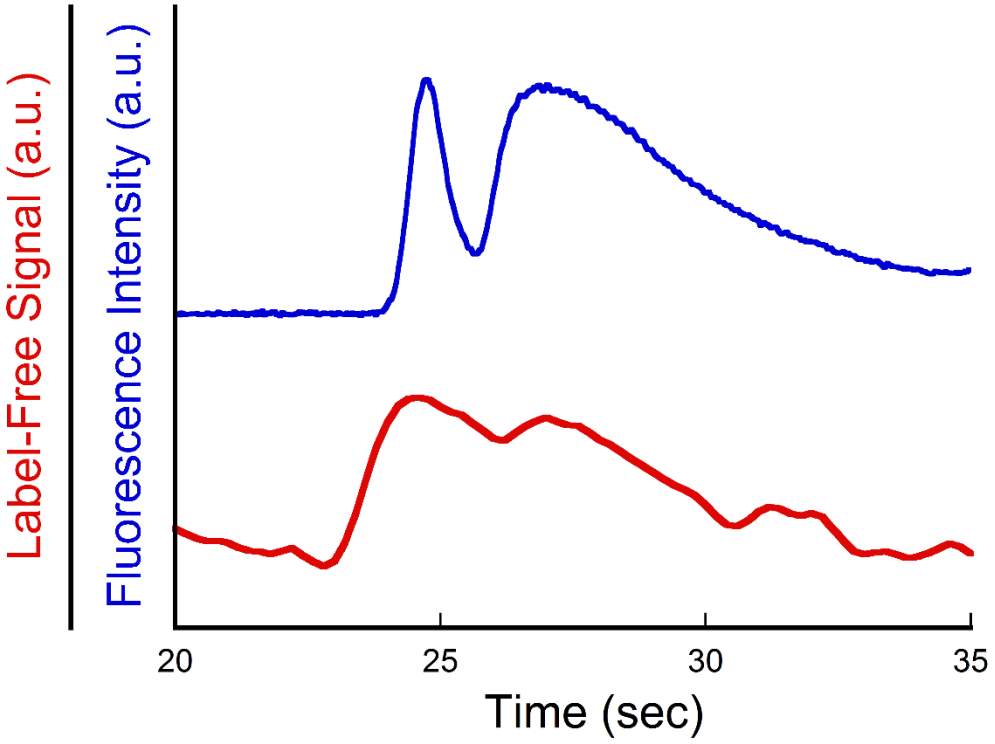

Figure 35. Comparison of fluorescence observation and label-free observation. For fluorescence observation, DNA was stained with YOYO-1 (dye-to-base, 1:150).

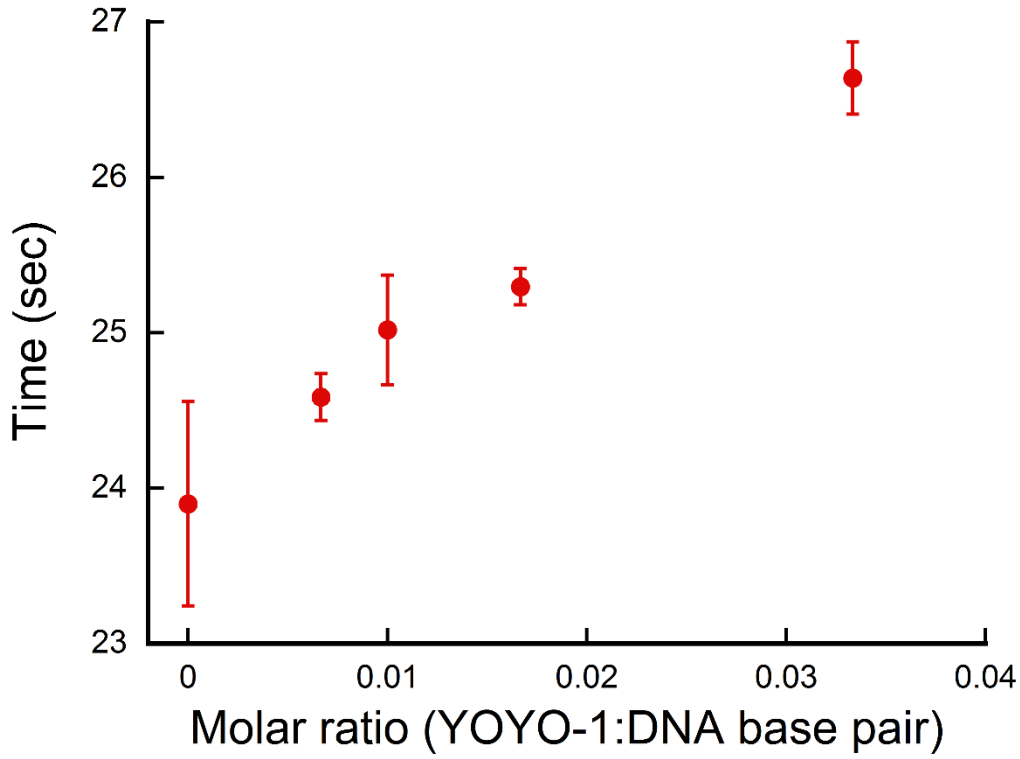

Figure 36. Peak arrival time of the 1 kbp DNA at various YOYO-1 concentrations. n = 3.

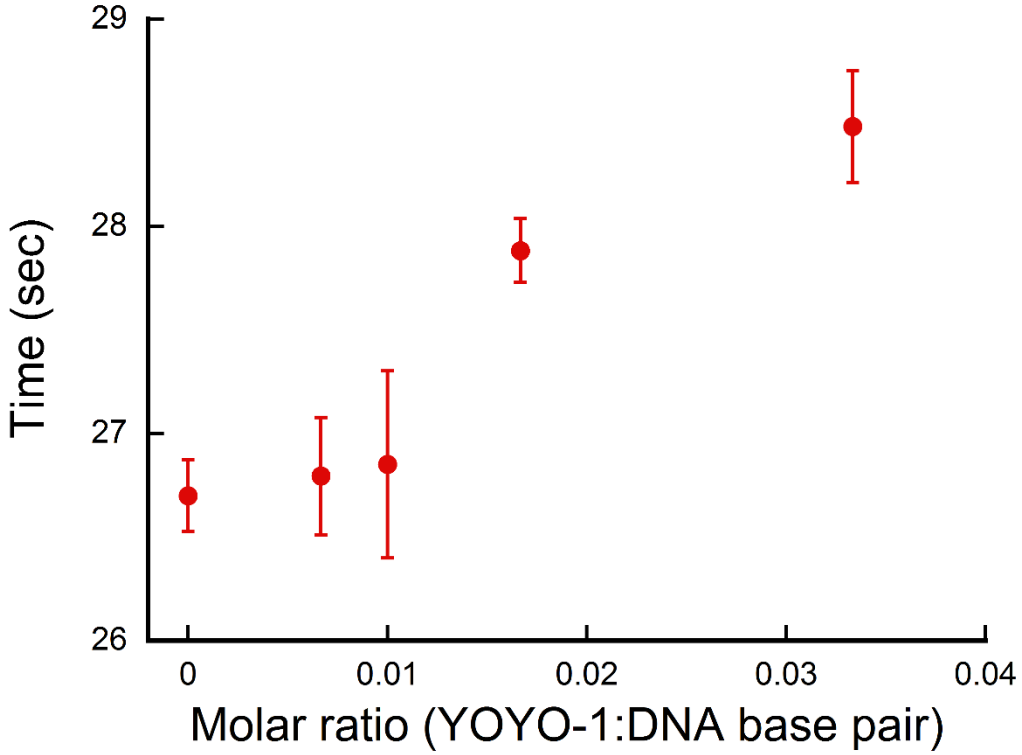

Figure 37. Peak arrival time of the 100 bp DNA at various YOYO-1 concentrations. n = 3.

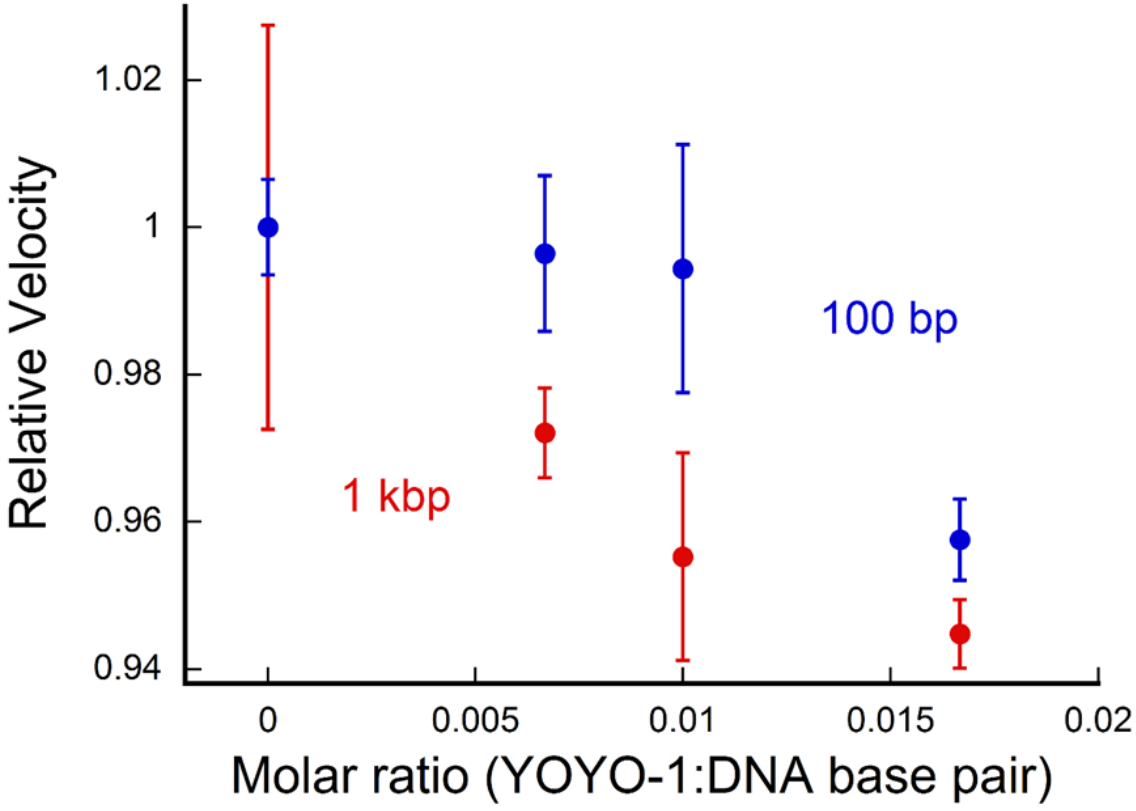

Figure 38. Effect of electrophoretic speed based on concentration (100 bp; blue, 1 kbp; red). n = 3.

4.4 Conclusions

In this study, we successfully monitored the separation of label-free DNA using nanopillar devices. It was possible to generate an electropherogram without fluorescence labeling using diffracted light derived from the periodic structure of the nanopillars. Although it was necessary to perform fluorescent labeling to observe the separation of biomolecules using the nanostructures, it is conceivable that changes in the molecular state such as effective charge and size (persistence length and contour length) accompanying the formation of a complex with the labeling reagents affects the separation. Separation by nanostructures can be observed without labeling bias using this measurement system. In this study, changes in molecular dynamics associated with fluorescent labeling were confirmed. Additionally, this change suggested that resolution of the separation decreases due to labeling. Although this method requires investigation for further enhancement of sensitivity and high throughput, we expect that further development of this system will provide a novel separation mechanism not only for DNA but also for proteins and amino acids. Additionally, this method possesses applicability as a tool for the label-free monitoring of the nanofluidics of various structures through the use of diffracted light derived from nanofluidics.

4.5 References

1. M. Orita, H. Iwahana, H. Kanazawa, K. Hayashi, T. Sekiya, *PNAS*. **86**, 2766−2770 (1989).
2. M. R. Shortreed, H. Li, W. H. Huang, E. S. Yeung, *Anal. Chem.*, **72**, 2879–2885 (2000).
3. K O Voss, H. P Roos, N J. Dovichi, *Anal. Chem*., **73**, 6, 1345-1349 (2001).
4. W. N. Vreeland, R. J. Meagher, A. E. Barron, Anal. Chem., **74**, 4328–4333 (2002).
5. Y. W. Lin, M. J. Huang, H. T. Chang, *J. Chromatogr. A*, **1014**, 47–55 (2003).
6. M. S. Rashed, P. T. Ozand, M. P. Bucknall, D. Little, *Pediatr. Res.*, **38**, 324−31 (1995).
7. M. Unlu, M. E. Morgan, J. S. Minden, *Electrophoresis*, **18**, 2071−2077 (1997).
8. I. M. Cristea, S. J. Gaskell, A. D. Whetton, *Blood*, **103**, 3624-3634 (2004).
9. J. Cao, H. B. Qu, Y. Y. Cheng, *Electrophoresis*, **31** (10) 1689– 1696 (2010).
10. A. W. Henkel, K. Müller, P. Lewczuk, T. Muller, K. Marcus, J. Kornhuber, J. Wiltfang, *J Neural Transm*, **119**, 779-788 (2012).
11. L. Wang, J. Wu, Q. Wang, C. He, L. Zhou, J. Wang, Q. Pu, *J. Agric. Food Chem*., **60**, 1613–1618 (2012).
12. R. L. Bieleski, N. A. Turner, *Anal. Biochem*., **17**, 278−293 (1966).
13. Z. D. Sandlin, M. Shou, J. G. Shackman, R. T. Kennedy, *Anal. Chem.*, **77**, 7702−7708 (2005).
14. I. Ilisz, A. Aranyi, A. J. Péter, *Chromatogr. A*, **1296**, 119– 139 (2013).
15. S. Vijayasarathy, P. Prasad, L. J. Fremlin, R. Ratnayake, A. A. Salim, Z. Khalil, R. J. Capon, *J. Nat. Prod*., **79**, 421– 427 (2016).
16. J. Kameoka, H. G. Craighead, H. Zhang, J. Henion, *Anal. Chem.*, **73**, 1935−1941 (2001).
17. J. Han, S. W. Turner, H. G. Craighead, *Phys. Rev. Lett.*, **83**, 1688−1691 (1999).
18. J. Han, H. G. Craighead, *Science*, **288**, 1026-1029 (2000).
19. N. Kaji, Y. Tezuka, Y. Takamura, M. Ueda, T. Nishimoto, H. Nakanishi, Y. Horiike, Y. Baba, *Anal. Chem*., **76**, 15−22 (2004).
20. J. Fu, J. Yoo, J. Han, *Phys. Rev. Lett.*, **97**, 018103 (2006).

21. J. Fu, R. B. Schoch, A. L. Stevens, S. R. Tannenbaum, J. Han, *Nat. Nanotechnol*., **2**, 121-128 (2007).
22. J. D. Cross, E. A. Strychalski, H. G. Craighead, *J. Appl. Phys*., **102**, 024701 (2007).
23. S. Pennathur, F. Baldessari, J. G. Santiago, M. G. Kattah, J. B. Steinman, P. J. Utz, *Anal. Chem*., **79**, 8316– 8322 (2007).
24. N. Laachi, C. Declet, C. Matson, K. D. Dorfman, *Phys. Rev. Lett.*, **98**, 098106 (2007).
25. P. Mao, J. Han, *Lab Chip*, **9**, 586– 591 (2009).
26. T. Yasui, N. Kaji, M. R. Mohamadi, Y. Okamoto, M. Tokeshi, Y. Horiike, Y. Baba, *ACS Nano*, **5**, 7775-7780 (2011).
27. Yasui, T.; Kaji, N.; Ogawa, R.; Hashioka, S.; Tokeshi, M.; Horiike, Y.; Baba, Y. Anal. Chem., **83**, 6635-6640 (2011).
28. S. G. Park, D. W. Olson, K. D. Dorfman, *Lab Chip*, **12**, 1463-1470 (2012).
29. T. Yasui, N. Kaji, Y. Okamoto, M. Tokeshi, Y. Horiike, Y. Baba, *Microfluid. Nanofluid.*, **14**, 961-967 (2013).
30. T. Yasui, S. Rahong, K. Motoyama, T. Yanagida, Q. Wu, N. Kaji, M. Kanai, K. Doi, K. Nagashima, M. Tokeshi, M. Taniguchi, S. Kawano, T. Kawai, Y. Baba, *ACS Nano*, **7**, 3029-3035 (2013).
31. S. Rahong, T. Yasui, T. Yanagida, K. Nagashima, M. Kanai, A. Klamchuen, G. Meng, Y. He, F. Zhuge, N. Kaji, T. Kawai, Y. Baba, *Sci. Rep.*, **4**, 5252-5259 (2014).
32. T. Yasui, N. Kaji, R. Ogawa, S. Hashioka, M. Tokeshi, Y. Horiike, Y. Baba, *Nano. Lett.*, **15**, 3445-3451 (2015).
33. S. H. Ko, D. Chandra, W. Ouyang, T. Kwon, P. Karande, J. Han, Nat. Nanotechnol., **12**, 804-812 (2017).
34. B. Kundukad, J. Yan, P. S. Doyle, *Soft Matter*, **10**, 9721-9728 (2014).
35. C. Carlsson, A. Larsson, M. Jonsson, *Electrophoresis*, **17**, 642-651 (1996**)**.

36. M. Eriksson, M. Mehmedovic, G. Westman, B. Akerman, *Electrophoresis*, 26, 524-532 (2005).

37. F. Dang, W. Li, L. Zhang, J. Mohammad, I. Tatsuhiro, H. Kiwada, N. Kaji, T. Manabu, Y. Baba,. *J. Chromatogr. A*, **1118**, 218–225 (2006).

38. S. Quake, H. Babcock, S. Chu, *Nature*, **388**, 151−154 (1997).

Chapter 5.
Concluding Remarks and Future Perspectives

In this thesis, the author constructed a novel label-free detection method based on the optical diffraction derived from lasers passed through a nanofluidic channel. Micro- and nanofluidic device that introduced solutions into a nanochannel were fabricated, and label-free detection of biomolecules was performed using these fabricated devices. The author considered utility and size of the nanostructures for sensitivity when developing this method. Additionally, integration of separation analysis was achieved by the use of nanopillar structures. Changes in the molecular state were confirmed to result from the formation of the complex with the labeling reagent. Summary of this each chapter is as follows.

Fabrication of Micro- and Nanofluidic Device (Chapter 2)

The devices were fabricated in two ways. Two types of devices based on fluid control methods were fabricated, and these included a pressure driven method and an electric field driven method. By using electron beam lithography techniques, high precision patterning of all structures was achieved. By combining laser interference lithography with general photolithography techniques, patterning the periodic structures within the microchannel at nearly the same accuracy as electron beam lithography was achieved. Although it is limited to the patterning of the periodic structure, the patterning time can be significantly shortened (~20 min → ~1 min). Additionally, this method is suited to mass production, as it can pattern multiple substrates simultaneously by expanding the laser spot size. The results of this study demonstrate that these techniques provide a useful method for micro- and nanofluidic device fabrication.

Label-Free Detection Using Micro- and Nanofluidic Device (Chapter 3)

The author constructed a method of detecting samples within channels by using diffracted light specific to the nanofluidic channel. This method is based on the diffraction efficiency changes accompanying the refractive index changes. The author optimized the dimensions of

nanostructures based on the simulation analysis, and this system could detect label-free DNA at the single molecule level. Additionally, it was possible to quantify label-free DNA using not only diffracted light from the slit-like diffraction grating, but also diffracted light from periodic cylindrical structures. This method is applicable for label-free detection in micro- and nanofluidic devices possessing various structures.

Separation Analysis Using a Nanopillar Device (Chapter 4)

DNA separation using a nanopillar device was successfully monitored using our label-free detection system. It was possible to generate an electropherogram without fluorescent labeling by using diffracted light from the periodic structures of the nanopillar. We confirmed that the dynamics accompanying complex formation changed by monitoring separation using nanopillars in the presence or absence of fluorescent labeling. Although further improvement to sensitivity is required, this method can be used as a tool for the development and monitoring of novel separation mechanisms.

As summarized above, the author constructed the label-free detection system based on optical diffraction. In this method, target molecules can be quantified merely by the introduction of a solution to the system. It is also possible to identify multiple targets without labeling through combination with separation analysis. Further improvement of sensitivity can be achieved by nanostructure optimization and improvement of the optical system (high intensity light source, heterodyne detection, etc.). It is likely that detection capability comparable to fluorescence detection can be achieved. The author believes that this detection system will provide a useful tool for monitoring various nanofluidics, including those applicable to separation analysis of biomolecules.

ACKNOWLEDGEMENT

I would like to express my great appreciation to Professor Manabu Tokeshi (Hokkaido University) for his kind guidance, constructive suggestions, simulating discussions and continuous encouragement. I would like to acknowledge Associate Professor Takao Yasui (Nagoya University), Associate Professor Hirofumi Tani, Assistant Professor Akihiko Ishida and Assistant Professor Masatoshi Maeki (Hokkaido University) for valuable suggestions and experimental instruction.

I would like to express my gratitude to all my collaborators I have worked with during these years, especially Professor Junji Nishii (Hokkaido University), Mr. Haruya Kasa (Nihon Yamamura Glass Co. Ltd.) for the help, valuable comments, and experimental instruction regarding laser interference lithography techniques, Mr. Hiroyuki Yamazaki, Mr. Daiyu Okafuji, and Mr. Masao Ando (Shin-Etsu Chemical Co. Ltd.) for the help with the bonding process of micro- and nanofluidic devices; Professor Takehiko Kitamori (Tokyo University), Associate Professor Kazuma Mawatari, Assistant Professor Kyojiro Morikawa (Tokyo University), and Associate Professor Yan Xu (Osaka Prefecture University) for their valuable comments and experimental instruction on the fabrication of the micro- and nanofluidic devices, Professor Yoshinobu Baba (Nagoya University), Professor Noritada Kaji (Kyusyu University), and Professor Akihide Hibara (Tohoku University) for valuable suggestions and experimental instruction, and Ms. Ryoko Kurishiba (Hokkaido University) for the help with SEM observation.

I also thank Professor Noboru Kitamura, Professor Toshifumi Sato, Professor Toshihiro Shimada, and Professor Kuniharu Ijiro (Hokkaido University) for their valuable discussions.

It should be emphasized that these studies in this thesis have required the support at in and outside the laboratory with Professor Tokeshi's laboratory member. Among this group, Kazuki Shimizu helped me with the fabrication of the device and Koki Hoshikawa helped me with the simulation analysis of the electric fields.

A part of this work was conducted at Hokkaido University and was supported by the “Nanotechnology Platform” program of the Ministry of Education, Culture, Sports, Science and Technology (MEXT), the Grant-in-Aid for JSPS Research Fellow and Hosokawa Powder Technology Foundation.

The author would like to thank Editage (www.editage.jp) for English language editing.

Finally, I express my deep appreciation to my family members. They have always encouraged and financially supported me and have, at times, also given me much needed advice concerning my studies.